Lab on a Chip

CRITICAL REVIEW

View Article Online
View Journal | View Issue

Cite this: *Lab Chip*, 2017, **17**, 209

Controllable synthesis of functional nanoparticles by microfluidic platforms for biomedical applications – a review

Junping Ma,[a] Simon Ming-Yuen Lee,[a] Changqing Yi*[bc] and Cheuk-Wing Li*[a]

Received 20th August 2016,
Accepted 3rd December 2016

DOI: 10.1039/c6lc01049k

www.rsc.org/loc

Nanoparticles have drawn significant attention in biomedicine due to their unique optical, thermal, magnetic and electrical properties which are highly related to their size and morphologies. Recently, microfluidic systems have shown promising potential to modulate critical stages in nanosynthesis, such as nucleation, growth and reaction conditions so that the size, size distribution, morphology, and reproducibility of nanoparticles are optimized in a high throughput manner. In this review, we put an emphasis on a decade of developments of microfluidic systems for engineering nanoparticles in various applications including imaging, biosensing, drug delivery, and theranostic applications.

1. Introduction

In recent decades, nanoparticles have drawn significant attention in biomedicine as a result of their unique properties in imaging, optoelectronics, catalysis, sensing and drug delivery. Although the properties of nanoparticles are highly related to their size and morphology, it is technically challenging in conventional batch processes to reproducibly fabricate nanoparticles with a desired size and shape with a small standard deviation.

In conventional batch process systems, nanoparticles are synthesized by nanoprecipitation,[1–4] sol–gel,[5–7] ultrasonic,[8,9] micro emulsion[10–13] and reduction methods,[14–17] with the synthetic mechanism well understood.[4,18–23] For example, the formation of most polymeric nanoparticles can be divided into three stages: 1) a nucleus is formed that consists of several polymeric monomers. 2) The nucleus grows by adding in more monomers through a diffusion-limited process. This process continues until the formation of a polymer corona on the surface of nanoparticles, which results in the formation of kinetically locked nanoparticles. 3) Nanoparticles reach equilibrium with an exterior monomer, as characterized by extremely slow changes in their size.[24]

Similarly, the processes of inorganic nanoparticle synthesis are divided into nucleation and growth[25–29] stages, and separation of nanoparticles before the agglomeration. During a batch nanoparticle synthesis, the nucleation, growth and agglomeration processes are inevitably occurring at the same time. It is due to the lack of control of mixing and separation during particle growth from agglomeration processes, resulting in a high batch-to-batch variation in both size and size distribution of nanoparticles. Furthermore, up-scaling a batch synthesis will aggravate the situation of insufficient mixing and mass transfer problems, which leads to a polydispersed population of nanoparticles having various physical and chemical characteristics.[30–33]

Since 1990s, a large amount of research efforts has been devoted to microfluidic synthesis of nanoparticles. In particular, continuous-flow microfluidic systems, in contrast to conventional batch systems, are widely studied due to their precise control, rapid heat and mass transfer, high mixing efficacy, large reaction interfaces, and compatibility with online analysis.[34–37] Within a microfluidic system, the stages of nucleation and growth of nanoparticle formation can be isolated as a function of distance away from the position where solution mixing takes place to achieve excellent control of the particle size, size distribution, morphology,[38,39] and thus increase in reproducibility.[40,41]

In this review, we present a decade of developments of nanoparticle synthesis in microfluidic systems. First, the different microfluidic flow systems employed for nanosynthesis will be introduced. Then, we emphasize the developments of microfluidic systems for engineering nanoparticles for various applications in imaging, biosensing, drug and gene delivery, and theranostic applications. Comparing with conventional batch synthesis,[30,37,42–44] the advantageous features of microfluidic synthesis, together with its current challenges, are summarized in Table 1:

[a] *State Key Laboratory of Quality Research in Chinese Medicine, Institute of Chinese Medical Sciences, University of Macau, Macau SAR, China. E-mail: cheukwli@umac.mo*
[b] *Key Laboratory of Sensing Technology and Biomedical Instruments (Guangdong Province), School of Engineering, Sun Yat-Sen University, Guangzhou, China. E-mail: yichq@mail.sysu.edu.cn*
[c] *Research Institute of Sun Yat-Sen University in Shenzhen, Shenzhen, China*

Table 1 Advantages and disadvantages/challenges of microfluidic platforms for the synthesis of nanoparticles[30,31,35,37]

Advantages	Disadvantages/challenges
■ Large surface to volume ratios ■ Low sample/solution consumption ■ Excellent manipulation of reagents ■ Sufficient mixing, a controllable residence time and reaction conditions ■ Sufficient mixing, a controllable residence time and reaction conditions ■ Kinetic study due to well controlled heat and mass transfer ■ Synthesis with high reproducibility ■ Nanoparticles with a tunable size and a narrower size distribution, leading to enhanced physical/chemical performance ■ Potential for streamlined synthesis by integration of multi-steps on a single chip ■ Potential for online characterization, real time optimization and feedback control	■ Many device substrates have poor solvent compatibility and are not resistant to high temperature ■ Susceptible to channel clogging, which may also alter mixing ■ Certain substrates (such as glass and silica) or molds (Su-8-based) are expensive and involve clean room facilities ■ Limited online characterization techniques ■ Difficult to subject to online purification and extraction ■ Labor intensive pre and post treatments (not fully automated)

2. Flow systems used in nanosynthesis

In general, most nanoparticles are synthesized in conventional bulk systems by altering the precursors into desired nanoparticles with the approaches of stirring, shaking and sonicating (Fig. 1a). In the past decades, flow systems used in nanosynthesis have become widely investigated due to their as before mentioned advantages. With respect to the reacting phases involved in microfluidic systems,[30,37,45] the devices can be divided into two catalogues, single-phase continuous flow and segmented flow microfluidic systems.

Single-phase continuous flow microfluidic systems

A single-phase continuous flow (Fig. 1b) system is the most widely used in microfluidics as it is a homogeneous system that offers simplicity and a versatile control of the flow, reagent, reaction time, and temperature. Nanoparticle synthesis in single-phase continuous flow microfluidic systems[35,46–49] is conducted either with a single or multiple miscible solvents and the reagents are mixed through diffusion in laminar flow streams. For most single-phase passive mixers that are designed to work at a low Reynolds number (<10), the primary mixing mechanism is molecular interdiffusion across laminar streams due to the absence of turbulence. The mixing time is quadratically related to the channel width and the flow ratio of the miscible flows.[50,51] The mixing time in a microfluidic channel can be estimated by the following equation:[51]

$$\tau_{\mathrm{mix}} \sim \frac{w_{\mathrm{f}}^{2}}{4D} \approx \frac{w^{2}}{9D}\frac{1}{(1+1/R)^{2}}$$

where D: diffusivity of the solvent, w_{f}: width of the focused stream, w: channel width, and R: the ratio of the flow rate between the polymeric stream and the total flow rate of solvent.

To incorporate a transverse component of the flow to improve mixing performance, chaotic advection can be triggered in microchannels by repeatedly folding and stretching fluidic streams such that they become exponentially thin by using a staggered herringbone mixer, which can lead to an exponential increase of the interface between two fluids to achieve fast mixing.[52] The small dimensions of a microchannel can greatly reduce the mixing time to even milliseconds in the nucleation stage of nanosynthesis.

In addition, nanoparticles can be continuously modified by adding new reagents along the reaction, compared to droplet-based microfluidic systems, which offer the advantages of continuous modification and multi-step synthesis. The single-phase continuous flow strategy is also highly scalable in a sense that throughput can be improved by conducting multiple reactions in parallel,[37] to synthesize a large amount of nanoparticles with high reproducibility. Recently, various nanoparticles have been fabricated in continuous single-phase flow microfluidic systems through self-

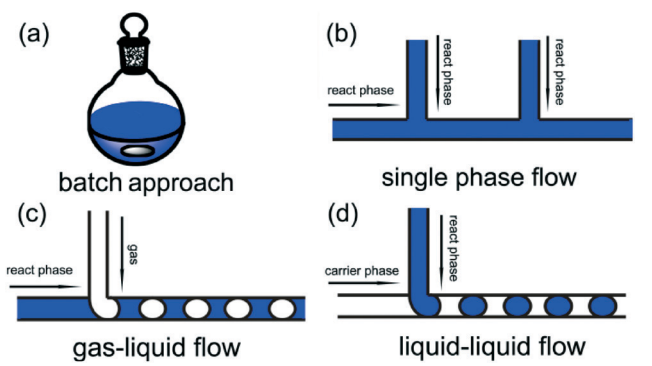

Fig. 1 Scheme of different processes to synthesize nanoparticles: (a) batch synthesis; (b) single-phase flow synthesis; (c) gas–liquid multiphase flow synthesis; and (d) liquid–liquid multiphase flow synthesis.

assembly and nanoprecipitation. T-junction,[24,46] capillary and coaxial tubes,[53] flow focusing geometry and micro mixing-based reactors are widely used in single-phase microfluidic systems.

Multiphase flow microfluidic systems

In contrast to a single-phase flow, a multiphase microfluidic flow, also known as a segmented flow, consists of two of more immiscible fluids or isolated phases.[54] By the addition of a new phase, a recirculation motion[55] is triggered to provoke stretching and folding of a solution that enhances the mixing efficiency just as chaotic advection in the absence of dispersion.[56] The multiphase flow synthesis approach also offers the advantage of narrowing the deviation of the residence time as the reactions are conducted in well-defined droplets. An additional advantage of a multiphase system is that direct contact of the liquid with the microchannel is prevented such that the risk of channel clogging caused by deposition of reactants/products on the channel surfaces[55,57–60] is minimized.

Multiphase flow synthesis can be divided into two sub-categories: gas–liquid flows (Fig. 1c) and liquid–liquid flows (Fig. 1d). In liquid–liquid two-phase flows, often presented as water-in-oil and oil-in-water dispersions, surfactants are often added to inhibit coalescence of the dispersed droplets.[61] The morphology of the droplets is closely related to the flow rate and chip design. Because of adequate mixing efficacy, quick heat and mass transfer in liquid–liquid flow systems, nanoparticles with versatile sizes and shapes are synthesized in a controlled manner in these systems.[34,44] Since the reacting solutions are encapsulated within liquid droplets, which significantly prevent contamination and channel clogging, nanoparticles can be synthesized with higher reproducibility. On the other hand, subsequent addition of agents in the encapsulated reacting solution is challenging as it is difficult to synchronize the merging of discrete droplets.[62] In gas–liquid systems, it is always present as a bubbly flow[63,64] dispersed in a continuous liquid phase. The introduction of a gas phase can significantly improve the mixing efficacy with the creation of recirculation.[37] One of the most attractive features of gas–liquid segmented flow reactors is the simple separation of the gas from the liquid[65,66] to obtain the desired nanoparticles. However, they still suffer from the possible clogging which can be avoided with liquid–liquid flow reactors.[30,62]

3. Application of nanoparticles synthesized by microfluidic systems

Nanoparticles for imaging

Nanoparticles are promising materials for fluorescence,[67] magnetic resonance and ultrasound imaging[68,69] because of their unique physicochemical properties. Their reduced dimensions offer a high surface area to volume ratio for surface modification with a wide range of functional groups which facilitates the development of multi-module imaging probes. Imaging performance is tightly linked to the size and size distribution of nanoparticles.[69,70] Due to the inefficient and uncontrolled mixing in the conventional bulk synthesis approach, it is a challenge to control the quality and reproducibility of nanoparticles. The use of microfluidic systems can precisely control the synthesis process thus improve the performance of imaging probes.

Magnetic nanoparticles are the popular candidates for on-chip nanofabrication, due to their attractive role as contrast enhancing agents in magnetic resonance imaging (MRI). Microfluidic platforms can efficiently optimize the parameters that strongly affect their physiochemical properties. Due to the small dimensions of microchannels in microfluidic systems that markedly improved the mass and heat transport, size control is achieved by scaling down the reactor dimensions. Hassan's group[71] has synthesized magnetic nanoparticles in a coaxial flow PDMS device (Fig. 2a) by co-precipitation of ferrous and ferric ions with

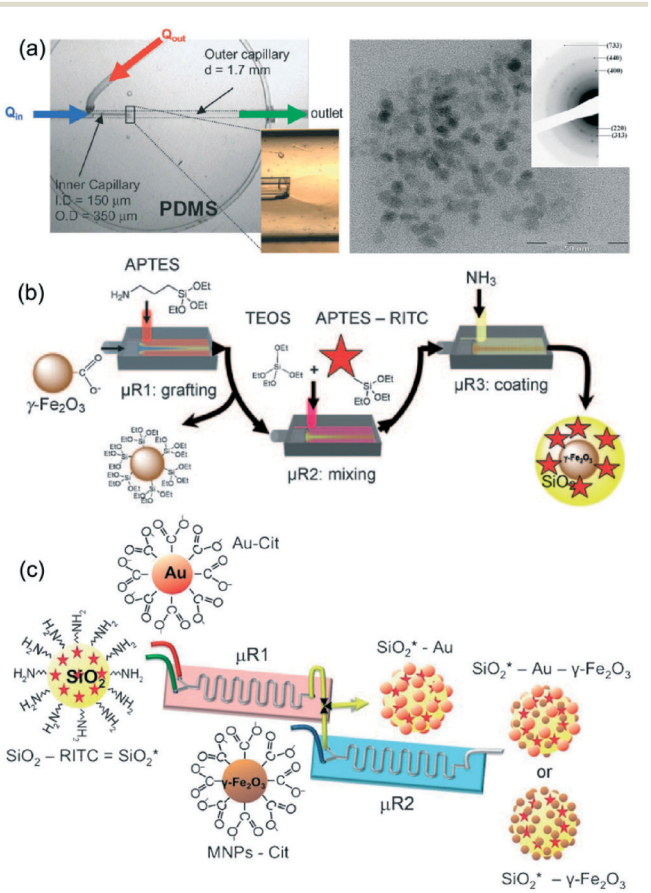

Fig. 2 (a) A 3D coaxial flow device for synthesis of magnetic nanoparticles by co-precipitation of iron(II) and iron(III), and a TEM image of nanoparticles fabricated in the device. Reproduced from ref. 71, copyright 2008 The Royal Society of Chemistry. (b) Scheme of the continuous flow synthesis of the fluorescent core/shell MNP/silica nanoparticles. Reproduced from ref. 48, copyright 2009 Wiley. (c) Scheme of the assembly of multifunctional nanoparticles with a two-step microfluidic process. Reproduced from ref. 78, copyright 2013 Wiley.

tetramethylammonium hydroxide (TMAOH) as the alkaline solution. The selection of TMAOH rather than other basic solutions is because the TMA^+ cations can enhance the stability of the nanoparticles. In order to avoid channel clogging, a 3D coaxial flow device has been designed to perform the mixing of two miscible solutions. TEM and vibrating sample magnetometer (VSM) results have indicated the success of on-chip synthesis of superparamagnetic iron nanoparticles with an average size about seven nanometers.

While it may take many hours in conventional bulk synthesis to obtain desired nanoparticles, the synthesis time can be significantly reduced with the help of microfluidic reactors. Hassan's group has further employed the mentioned 3D coaxial flow device with a microtubular aging coil and a 60 °C water bath to fabricate magnetic nanoparticles with separated nucleation and aging processes.[72] The aging coil can accelerate the transformation process of the ferrihydrite phase into goethite within 15 minutes with a smaller size, in contrast to the several hours required under conventional batch conditions. Their group has also synthesized fluorescent and magnetic nanoparticles in a continuous multistep microfluidic device[48] (Fig. 2b). The construction of fluorescent silica-coated magnetic nanoparticles (FSMNPs) has been conducted in three separate microreactors: 1) to conjugate 3-aminopropyltriethoxysilane (APTES) onto citrate-conjugated nanoparticles; 2) to add and mix silica precursors, such as tetraethyl orthosilicate (TEOS) and dye-conjugated APTES; and 3) to modify the nanoparticles with silica. The synthesized FSMNPs can be applied to magnetic resonance imaging (MRI) and fluorescence imaging. Further online modification and online detection can be carried out in the on-chip synthesis.

Microfluidic systems offer the convenience of controlling various experimental parameters including the concentration, temperature, reaction time and velocity to optimize the formation of nanoparticles.[73–77] Hassan's group[78] has prepared a lab-on-a-particle construct by self-assembly of fluorescent compound-doped silica nanoparticles, gold nanoparticles and magnetic nanoparticles through continuous multistep microfluidic systems (Fig. 2c). The assembly processes in microfluidic systems are dynamic and the kinetics is controlled by the hydrodynamic conditions, including the rate of shear flow and residence time to obtain desired structures. The microfluidic systems consist of two Y-shaped glass microreactors to modify gold nanoparticles and magnetic nanoparticles on silica nanoparticles through self-assembly. The characterization results have showed the potential of microfluidics in nanoparticle synthesis for imaging purposes. Jiao *et al.*[79] have prepared PEGylated Fe_3O_4 nanoparticles through a microfluidic system by pyrolysis of ferric acetylacetonate ($Fe(acac)_3$) in anisole with PEG and oleylamine at 250 °C. The effects of velocity, residence time, tube reactor dimensions, and concentration on the particle size distribution are investigated.

Moreover, microfluidic systems can synthesize nanoparticles with smaller size and smaller polydispersity than those prepared using conventional bulk synthesis, thanks to their better control of the reaction conditions. Frenz *et al.*[80] have synthesized magnetic nanoparticles in a droplet-based microfluidic system, wherein precipitation occurred in milliseconds and fusion of droplet pairs by electro-coalescence is well controlled and reproducible. The pairing droplets have been generated in a robust and flexible PDMS device by two aqueous phases emulsified by FC-40 oil; paired droplets coalesced with the addition of voltage between the two electrodes. The smallest size of synthesized magnetic nanoparticles is 4 nm, which is similar to the smallest dimension achievable by other off-chip approaches.

Many dye-doped nanoparticles and quantum dots have been prepared for fluorescence imaging. Compared with conventional fluorescent agents, nanoparticles exhibit high stability against photobleaching, with the excitation and emission spectra tunable in a narrow range. However, it is difficult to achieve reproducible nanoparticle fabrication by conventional bulk synthesis because mixing and nucleation parameters are not well controlled. The use of microfluidic systems, together with online characterization, allows better control of governing parameters, which significantly improves the reaction efficacy and controllability. Wacker *et al.*[67] have synthesized fluorescent silica nanoparticles by the Stöber method in a droplet-based PDMS microfluidic chip. The size of fluorescent SiO_2 nanoparticles can be well controlled in a wide range and photobleaching of these nanoparticles is slower than that of fluorescein isothiocyanate in water. Liu *et al.*[68] have prepared size and surface chemistry-controlled supramolecular nanoparticles by regulating the ratios of reagents with high flexibility and reproducibility in a PDMS microfluidic chip for molecular imaging. Supramolecular nanoparticles with different sizes and surface chemistries can be obtained with a narrow size distribution and subsequent evaluation of the cellular uptake efficiency of nanoparticles has showed strong correlation to the size and surface properties. Kovalenko and co-workers[81] have synthesized cesium-based nanoparticles in a droplet microfluidic system, which was integrated with online photoluminescence and absorption characterization. When compared with conventional bulk synthesis, the reagent consumption and screening time are greatly reduced.

Another imaging technology that leverages the advantages of nanoparticles is ultrasound imaging. Ultrasound imaging is a low-cost, safe and non-invasive technology, albeit suffers from its low contrast. Microbubbles and nanobubbles with large impedance mismatches can enhance the contrast thus are widely used in diagnosis. Generally, it is complicated and laborious to fabricate functionalized bubbles by the conventional approach, and the synthesized bubbles have a broad size distribution in the absence of precise condition monitoring. Microfluidic systems have demonstrated efficient, single-step methods for the synthesis of functionalized bubbles with an improved size distribution and stability. Park *et al.*[82] have produced multifunctional nanoparticle-functionalized bubbles with a low polydispersity index and high stability *via* a

single-step approach in a microfluidic device. The bubbles are generated by flow focusing in a PDMS microfluidic device with height, width and length of 120 μm, 50 μm and 260 mm, respectively. The central channel is filled with CO_2 with a pressure of 48.3 kPa, while the two side channels are loaded with an aqueous solution consisting of lysozyme, alginate and nanoparticles (magnetic nanoparticles, gold nanoparticles or SiO_2-encapsulated CdSe/ZnS nanoparticles). The synthesized nanoparticle-functionalized bubbles have showed enhanced contrast in ultrasound imaging and can serve as a multiple imaging agent. Peyman *et al.*[69] have presented the generation of lipid-stabilized nanoparticles encapsulated by perfluorocarbons, so called nanobubbles, through a new microfluidic method. The concentration of the nanobubbles is as high as 10^{11}–10^{12} nanoparticles per mL, and the particles have showed excellent stability with little changes over seventeen days of storage. Moreover, the nanoparticles have showed higher resolution contrast than a mixture of macro and nanosized imaging agents, and the *in vitro* and *in vivo* results have indicated the higher contrast intensity for the microfluidics-synthesized nanobubbles.

Nanoparticles for biosensing

Nanoparticles with unique physical and chemical properties can also serve as biosensors.[83–91] Since these properties depend on the characteristic size and shape of nanoparticles, a broad detection range is achievable by delicate control of nanosynthesis. Furthermore, the high surface-to-volume ratio of nanoparticles can significantly improve the sensing sensitivity when compared with bulk materials.

Recently, metal nanoparticle-based biosensors have received a lot of attention in their fabrication and applications.[92–96] These biosensors are based on the localized surface plasmon resonance (LSPR) phenomenon of metal nanoparticles. Surface plasmons (SPs) are defined as "coherent oscillations of conduction electrons on a metal surface excited by electromagnetic radiation at a metal–dielectric interface" by Nuzzo's group.[97] LSPR is the result of the restriction of a surface plasmon in a nanoparticle of size commensurate with or smaller than the wavelength of light applied to excite the plasmon.[98] Due to the resonant oscillation of free electrons of noble metal nanoparticles in the presence of light, the refractive index changes including a large shift in the plasmon angle, broadening of plasmon resonance, and an increase in the minimum reflectance,[99] resulting in the enhancement of optical and photothermal properties. Silver[53,58,59,100–105] and gold nanoparticles[25,26,29,60,106–117] are the most common nanoparticles synthesized for LSPR, and the synthesis of other metal nanoparticles such as Pt and copper also has been attempted. Investigations into the synthesis of noble metal nanoparticles have received considerable attention.

The LSPR frequency of metal nanoparticles is highly associated with the size, shape, dielectric properties, aggregate morphology, surface modification, and refractive index of the surrounding medium.[95,118] It is also worth noting the importance of developing anisotropic metal nanoparticles as they offer promising shape-dependent optical characteristics that are absent in their spherical NPs counterpart. For example, gold nanorods exhibit multiple absorbance bands that vary with the aspect ratio in the UV-vis-NIR absorption spectrum, while a single band is observed in gold nanospheres.[119] Other anisotropic metal nanorods and nanowires have exhibited enhanced electric fields and surface enhanced signals when compared to spherical NPs made from the identical material, which provided fascinating opportunities for biosensing.[17]

Kinetic control and selective surface passivation are the mechanisms involved in the major approaches of gold nanoparticle formation.[118] To synthesize gold nanoparticles with different shapes, the capability to fine-tune multiple parameters, such as the reduction potentials of metal complexes, reagent concentration, and adsorbate binding strength, is essential. Under the kinetic control approach, the shape of the nanoparticles is directed by the overall reduction rate of metal ions, in which a slow reduction rate of Au^+ favours the formation of fewer facets on the nanoparticles. By using an appropriate adsorbate, like Ag, some facets of Au are blocked by the adsorbate thus resulting in the generation of different shapes. This type of selective surface passivation approach is also affected by the reagent concentration and adsorbate binding strength. Because the rapid reaction kinetics of nanoparticle synthesis is closely interrelated with mixing efficiency and reagent addition,[44,116] it is difficult to achieve delicate control in conventional bulk synthesis. Moreover, challenges including the reproducibility, reliability, scalability still remain to be overcome before these metal nanoparticles can be translated for clinical uses.

Integration with online analysis is another technical challenge in conventional bulk synthesis. In contrast, the capabilities of microfluidic systems, which enabled precise control of mixing and separation during the nucleation and growth processes of nanoparticle fabrication, guarantee high reproducibility, reliability, and scalability. It is also easy to integrate online biosensing analysis modules with microfluidic devices to improve sensing efficacy.

The first synthesis of silver nanoparticles in microfluidics was carried out in a continuous single flow tubular microreactor with silver pentafluoropropionate as a precursor in isoamyl ether[53] (Fig. 3a). Trioctylamine was chosen as the surfactant as a result of its high solubility in the reactant phase. Silver nanoparticles were fabricated rapidly by thermal reduction within minutes in the microfluidic system. The silver nanoparticles were smaller in size and narrower in size distribution than those prepared with bulk synthesis. The first microfluidic synthesis of gold nanoparticles was also conducted in a continuous single flow microreactor,[120] where gold nanoparticles (15 to 24 nm) were fabricated by a seeding growth approach: the gold salt $HAuCl_4$ was reduced with ascorbic acid in the presence of 12 nm citrate-stabilised gold seeds. The optimization of the synthetic parameters, such as

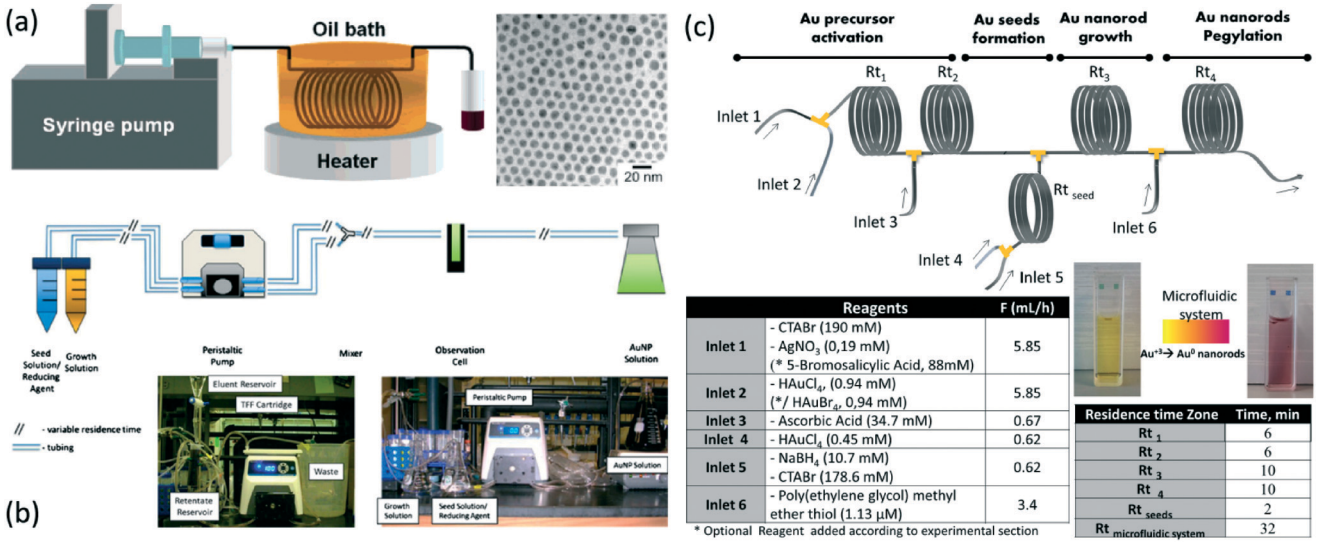

Reagents		F (mL/h)
Inlet 1	- CTABr (190 mM) - $AgNO_3$ (0,19 mM) (* 5-Bromosalicylic Acid, 88mM)	5.85
Inlet 2	- $HAuCl_4$, (0.94 mM) (*/ $HAuBr_4$, 0,94 mM)	5.85
Inlet 3	- Ascorbic Acid (34.7 mM)	0.67
Inlet 4	- $HAuCl_4$ (0.45 mM)	0.62
Inlet 5	- $NaBH_4$ (10.7 mM) - CTABr (178.6 mM)	0.62
Inlet 6	- Poly(ethylene glycol) methyl ether thiol (1.13 μM)	3.4

* Optional Reagent added according to experimental section

Residence time Zone	Time, min
Rt_1	6
Rt_2	6
Rt_3	10
Rt_4	10
Rt_{seeds}	2
$Rt_{microfluidic\ system}$	32

Fig. 3 (a) Illustration of a tubular microreactor for synthesis of Ag nanoparticles and the transmission electron microscopy (TEM) image of microfluidics-synthesized silver nanoparticles under the conditions of a temperature of 100 °C and a flow rate of 0.08 mL min^{-1}. Reproduced from ref. 53, copyright 2004 The American Chemical Society. (b) The integrated device for the synthesis and functionalization of Au nanoparticles. Reproduced from ref. 106, copyright 2013 The American Chemical Society. (c) Multi-stage seedless synthesis of PEG-functionalized gold nanoparticles. The reagent composition and flow rates of each inlet and the corresponding residence times are presented. Reproduced from ref. 107, copyright 2016 Elsevier.

the flow rates and concentration ratios, were convenient in the microfluidic system, achieving gold nanoparticles of different sizes. Then gold nanoparticles with diameter ranging from 5 to 50 nm were obtained by direct reduction of $HAuCl_4$ with ascorbic acid in a single-phase continuous flow microreactor by the same group.[29] The gold nanoparticles were synthesized with a two times narrower size distribution than those prepared with bulk synthesis.

Continuous single flow synthesis offers fine tuning and convenience in adding new agents for multistep reactions. Murphy's group[106] has demonstrated a simple millifluidic reactor constructed from commercial components that are available in most labs for high throughput hydrophilic functionalized gold nanoparticles (Fig. 3b). This reactor can be tailored to prepare gold nanoparticles with a controlled size and shape (nanorods and nanocubes) with a high yield. In addition, the system has been integrated with tangential flow filtration and UV-vis absorbance spectroscopy to monitor in real time and to analyse the purity of gold nanoparticles as quality control. This reactor has provided a blueprint for the synthesis of versatile and functionalized metal nanoparticles for LSPR. Santamaria's group[107] has synthesized and functionalized gold nanoparticles through a multistep continuous single-phase microfluidic platform (Fig. 3c). This system has integrated gold precursor activation, gold seed formation, the growth and PEGylation of gold nanorods into a single platform with the flexibility to control each stage separately. By a one hundred fold reduction of PEG consumption, the nanoparticles synthesized in this microfluidic system still managed to have a higher stability than those prepared by bulk synthesis, while the overall synthesis cost should be greatly reduced. Besides, fine tuning the concentration of halide ions at different stages of the synthesis process realizes the control of the aspect ratio in nanorod formation. SadAbadi and co-workers[121] have *in situ* synthesized gold nanoparticles and integrated them into PDMS microdevices to serve as a LSPR-based biosensor for the detection of proteins and polypeptides. The microfluidics-synthesized nanoparticles have demonstrated 8.3 times improvement in the polydiversity of the size distribution. The integrated device presents high sensitivity and an extremely low detection limit as low as 185 pM, which shows potential in clinical applications. The shape of the nanoparticles is highly associated with their performance, while a few methods have been studied to control the shape of the nanoparticles. Fayad's group[122] presented a facile method for the synthesis of shape-tunable tetrathiafulvalene–gold hybrid nanoparticles *via* a 3D microfluidic chip in a single step.

Segmented flow microfluidic systems are an another common approach for the synthesis of plasmonic nanoparticles because they can effectively enhance the mixing and transverse transport of species, thus improving the size distribution of nanoparticles. It also hinders the direct contact between the liquid and the surface of the microchannel thus reduces the risks of nanoparticle absorption and channel clogging. Khan's group[44] has demonstrated the possibility of preparing anisotropic gold nanocrystals in a multiphase microfluidic system. The gold seeds and growth solution were dispensed into monodisperse droplets, which successfully prevented wall deposition of reactants during a twelve hour synthesis. It has also been shown that by on-chip tuning the reagent concentration and feed ratio, nanoparticles with various shapes (having various optical resonances) can be obtained for biomedical applications. Duraiswamy[116]

presented a robust, scalable, automated and reproducible synthesis process to manufacture thin gold nanoshells and nanoislands on colloidal silica surfaces. This continuous metal nanoparticles synthesis provides a bridge that integrates multiphase microfluidics and colloidal synthesis. Zhang *et al.*[102] have demonstrated a robust approach to synthesise Ag nanoparticles with controlled sizes and shapes in a gas–liquid droplet microreactor. The air segments were not only useful to produce the reducing agent, but also served to block both the homogeneous nucleation and evolution of single-crystal seeds into twinned nanoparticles.

Binary noble metal nanoparticles have been synthesized for LSPR at different optical channels. Knauer *et al.*[57] have synthesized noble metal nanoparticles with core/shell and multi-shell structures with a two-step microreactor. The average size and full width at a half maximum (FWHM) of Au/Ag core/shell and Au/Ag/Au multi-shell nanoparticles are 19.9 nm and 3.8 nm and 45.6 nm and 7.3 nm, respectively. The spectral position of LSPR of the nanoparticles has exhibited drastic shifts with the variation of the shell of nanoparticles. The drastic change in optical characteristics of binary noble metal nanoparticles synthesized using the micro segmented flow method should have promising potential for plasmonic applications. Copper is another choice to prepare metal nanoparticles with surface plasmon resonance. Xu *et al.*[123] have synthesized copper nanoparticles with a metal solution being reduced by sodium borohydride in a T-shaped microfluidic system. The size of copper nanoparticles increased with the increase in the flow rate, and the surface plasmon resonance absorptions have slightly blue-shifted.

Zinc oxide nanoparticles[124] are widely used in a range of sensing devices such as diodes,[125] gas sensors[126] and ultraviolet detectors.[127] On-chip synthesis of zinc oxide nanorods has been employed for sensing carbon monoxide (CO) and ammonia (NH_3) gases by Khoang and co-workers.[90] The detector responses to target gases are examined with the growth time of zinc oxide nanorods and six hours of growth presented the highest response to the gases. On-chip synthesis of zinc oxide nanowires as ultraviolet detectors was demonstrated by Silva's group,[87] showing significant improvement in sensing sensitivity, the response time and the recovery time.

Aminopropyl-functionalized silica–titania nanoparticles have been fabricated in multistep microfluidic devices for humidity sensing by Shiba and co-workers[85] (Fig. 4a). In the process of nanoparticle synthesis, the nucleation of titania is well controlled. Since the hydrolysis of TEOS is slower, the silica will condense on the titania nuclei to form core–shell silica–titania nanoparticles. The synthesized nanoparticles have a size of about 33 nm with a narrow size distribution

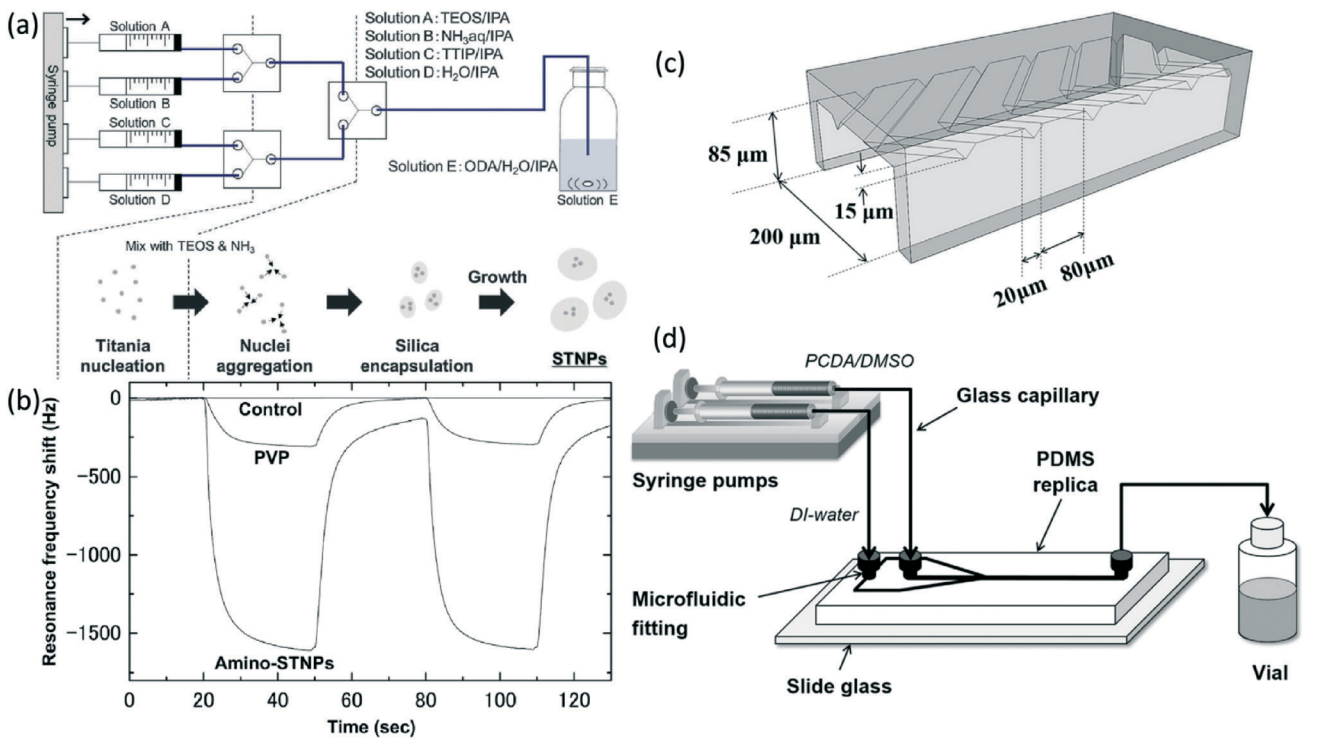

Fig. 4 (a) A microfluidic system for the synthesis of silica/titania-based nanoparticles by the controlled nucleation-induced growth method. (b) Resonance frequency shift of the nanoparticle-coated quartz crystal microbalance used to sense dry nitrogen gas containing water vapor. Reproduced from ref. 85, copyright 2015 The Royal Society of Chemistry. (c) Schematic three-dimensional view of the staggered herringbone micromixer microchannel. (d) Experimental setup for synthesis of nanoparticles in the staggered herringbone micromixer microfluidic chip. Reproduced from ref. 88, copyright 2016 Elsevier.

and highly stability, and have showed great responses to water vapour when compared to commercial PVP (Fig. 4b).

Polydiacetylene (PDA) is an excellent material to serve as a multipurpose sensor as its colour changes in response to various stimuli such as solvent, pH, temperature, specific molecular recognition and external force. Kim's group[88] has synthesized PDA nanoparticles with size ranging from 36 to 86 nm in a PDMS-based staggered herringbone micromixer (SHM) (Fig. 4c and d). With the size controlled by adjusting the Reynolds number, the microfluidic synthesis exhibited high reproducibility. Compared to hydrodynamic focusing, the yield of microfluidic synthesis using SHM is 40 times higher.

Nanoparticles for drug delivery

Biodegradable polymeric nanoparticles have been widely used for drug delivery,[128] due to their enhanced therapeutic and decreased side effects.[129] Moreover, many conventional methods are still suffering from poor drug loading efficacy and lack of flexibility to fine tune the fabrication parameters. Microfluidic systems offer the ability to synthesize nanoparticles[49,130–151] with a narrow size distribution,[40,46,147,152] improved reproducibility,[153] and high encapsulation efficiency[48] and these systems are integrated with high flexibility and online analysis of the fabrication processes. Some of the advantages of nanosynthesis in microfluidic platforms for drug and gene delivery are also covered in recent reviews.[154,155]

Farokhzad's group has firstly synthesized drug loaded polymeric nanoparticles by a flow force microfluidic device[24] (Fig. 5a and b). Nanoparticles can be prepared by precipitation of drug and polymer precursors from an organic to a non-solvent in a hydrodynamic flow focusing chip made of PDMS. This simple and robust approach has been adopted by many researchers to synthesize various nanoparticles for drug delivery. The size and size distribution of nanoparticles can be controlled through factors like the flow rate, precursor composition and concentration of reactants. This microfluidic synthesis approach offers high flexibility for optimization which significantly accelerates the development of polymeric nanoparticles for therapy. Then, the same group has developed a drug delivery system which simultaneously loads cisplatin and docetaxel with distinct solubilities inside the polymeric nanoparticles[136] (Fig. 5c and d). The prodrug polylactic acid (PLA)–Pt(IV), block polymer PEG–PLGA, and docetaxel are blended and dissolved in acetonitrile to facilitate self-assembly of the dual drug loaded nanoparticles in the microfluidic system and subsequently are modified with A10 RNA aptamer, the targeting ligand. The microfluidics-synthesized nanoparticles have smaller sizes, a narrow size distribution, and higher drug loading capabilities than the nanoparticles fabricated in bulk approaches. Santos's group[40] has developed a glass capillary-based microfluidic platform to synthesize various nanoparticles by 3D coaxial flows with high productivity.

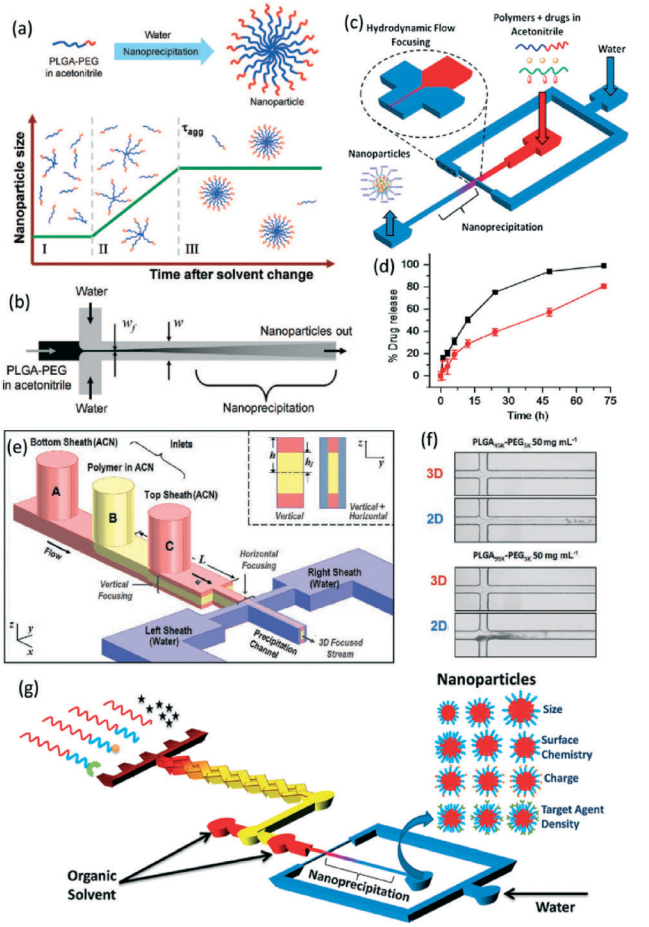

Fig. 5 (a) Scheme of the process of nanoprecipitation of PLGA–PEG copolymers. (b) Rapid mixing and nanoprecipitation in a microfluidic chip to synthesize polymeric nanoparticles. Reproduced from ref. 24, copyright 2008 The American Chemical Society. (c) Synthesis of drug loaded polymeric nanoparticles in a flow forcing microfluidic chip. (d) *In vitro* release of encapsulated platinum (circle) and docetaxel (square) in PBS at 37 °C from NPs. Reproduced from ref. 136, copyright 2010 National Academy of Sciences of the United States of America. (e) Three-dimensional HFF microfluidics which could focus in both horizontal and vertical orientations to reduce clogging when fabricating nanoparticles. (f) Comparison of the clogging with 3D and 2D HFF microfluidic chips to form PLGA–PEG NPs with different molecular weights of PLGA. Reproduced from ref. 46, copyright 2011 Wiley. (g) Schematic of a microfluidic system with multi-inlet to synthesise a library of NPs. Reproduced from ref. 144, copyright 2013 The American Chemical Society.

Microfluidic platforms offer high flexibility to tailor a device for the fabrication of a particular type of nanoparticles. It is found that block polymers of high molecular weight such as polyethylene glycol–poly (lactic-*co*-glycolic acid) (PEG–PLGA) tend to clog the microchannels in two-dimensional hydrodynamic flow focusing (HFF) devices, and monodisperse nanoparticles cannot be synthesized in both 2D HFF and the bulk process.[46] Thus, three-dimensional HFF microfluidics are proposed to sheath starting materials in both horizontal and vertical orientations to minimize their contact with microchannel surfaces[46] (Fig. 5e and f). As a result, smaller and highly monodispersed nanoparticles can be

prepared by 3D HFF. In order to increase the speed of nanoparticle optimization and accelerate the clinical translation, Farokhzad's group[144] has designed a microfluidic platform that uses multiple precursors to optimize nanoparticles with a controlled size, surface chemistry, charge, drug encapsulation, and target agent density (Fig. 5g). When compared with the mentioned microfluidic systems, the superiority of this microfluidic platform is in the programmable mixing of the multiple precursors ahead of nanoprecipitation, thus significantly shortening the time required for optimization. 45 kinds of PEG–PLGA nanoparticles with different sizes and surface modifications are synthesized for *in vitro* and *in vivo* investigation of nanoparticle properties.

Lipid–polymer nanoparticles have gained increasing interest for drug delivery because of their high flexibility and biocompatibility.[156] However, it is too complex and laborious to synthesize controlled lipid–polymer nanoparticles in bulk approaches.[157] Microfluidic systems integrated with the precise flow control and HFF have been applied to fabricate size-tunable lipid–polymer nanoparticles. Jiang's group[132] has designed a two-stage, high throughput microfluidic chip to fabricate monodisperse lipid–polymer nanoparticles with a controlled size. The core of the nanoparticles is a PLGA polymer and the shell consists of dipalmitoyl phosphatidylcholine (DPPC), 1,2-distearoyl-*sn-glycero*-3-phosphoethanolamine-*N*-poly(ethylene glycol) (DSPE-PEG), and cholesterol. It has been shown that the higher the flow rate, the better is the mixing performance, which leads to smaller sized nanoparticles and lower PDI in the microfluidic platform. Another example is the synthesis of same size lipid–polymer nanoparticles featured with either a monolayer or a bilayer of a lipid shell in a two stage microfluidic device to study the effect of the shell structure on flexibility-regulated cell–nanoparticle interactions.[151] Hybrid Janus-like vesicles have been fabricated in a HFF PDMS microfluidic chip for controlled release of payloads.[149] The vesicles are a result of self-assembly of a mixture of PEO_{45}-*b*-PS_{45} block copolymer modified platinum nanoparticles and gold nanorods, and drug molecules. In the presence of H_2O_2 and the irradiation of near infrared (NIR) light, the encapsulated components will leak from the vesicles due to the photothermic effect of gold nanorods. The glass capillary-based microfluidic system has also received considerable attention because of its excellent solvent resistance and hydrophilic surface properties that efficiently inhibited aggregation of nanoparticles on the channel walls.

Nanoparticles have been widely applied in drug and gene delivery.[152,158–161] Microfluidics-synthesized nanoparticles have showed enhanced loading efficacy and stability. Belliveau *et al.*[158] have fabricated lipid nanoparticles for the delivery of small interfering RNA (siRNA) by an SHM-featuring microdevice. The synthesized nanoparticles have a size ranging from 20 to 100 nm, narrow size distribution (the PDI can be as low as 0.02), high loading efficiency and enhanced stability and scalability when compared to conventional fabrication processes. Chitosan-based nanoparticles are also fabricated in a microfluidic device for oligodeoxynucleotide delivery.[159] The cellular uptake performance and immunostimulatory responses are improved together with size distribution, loading efficiency and stability. Jiang's group[152] has constructed vesicles for the co-delivery of a hydrophilic drug and siRNA with a three-stage microfluidic chip. The loading efficiency of doxorubicin (DOX) and siRNA is as high as 96.6 ± 1.1% and 91.23 ± 4.51%, respectively. An *in vivo* study using a multidrug resistant tumour model has suggested the strong inhibition effect of the DOX and siRNA loaded vesicles. Wang's group[161] has developed a microfluidic platform (Fig. 6) to prepare and screen multifunctional supramolecular nanoparticles for the co-delivery of genes and proteins. The proteins, genes, functionalized ligands and scaffold modules can be optimized through the microfluidic platform consisting of two microfluidic chips. The microfluidic platform is a useful tool to customize and optimize nanoparticles for drug and gene delivery.

Nanoparticles for theranostics

Theranostics is an emerging field about "the combination of diagnostic and therapeutic capabilities into a single agent".[162] Theranostic nanoparticles are expected to monitor and provide treatment to diseases, *e.g.* cancer, simultaneously.[162,163] The diagnostic technologies include MRI, optical imaging, computed tomography (CT), position emission tomography, and ultrasound imaging. The therapeutic aspect is manifested by the use of drugs, genes and proteins. Microfluidic systems have contributed to this field because of their multi-step flow control capability to form multifunctional nanoparticles bearing therapeutic and diagnostic agents with

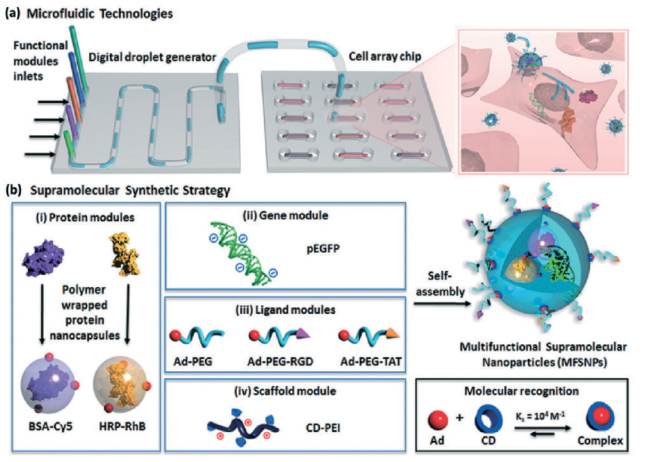

Fig. 6 (a) Microfluidic systems for synthesis and screening of multifunctional supramolecular nanoparticles. (b) A supramolecular synthetic strategy to form combinatorially serialized nanoparticles consisting of one or more parts of the four functional modules: i) proteins, ii) genes, iii) ligands (Ad–PEG, Ad–PEG–RGD, and Ad–PEG–TAT), and iv) a scaffold. Reproduced from ref. 161, copyright 2016 Wiley.

higher drug encapsulation than those prepared with conventional bulk methods.[122,164–170]

Multifunctional polycaprolactone (PCL) microencapsulated magnetic nanoparticles, CdTe quantum dots and tamoxifen have been fabricated in PDMS-based microfluidic chips in a single continuous step.[164] The synthesized particles have integrated magnetic targeting, fluorescence imaging and controlled drug release capabilities with a uniform size, reproducibility and scalable production. Microfluidic systems are also utilized to fabricate nanoparticle-incorporated microbubbles which consist of multiple imaging agents and therapeutic agents for diagnosis and treatment.[166]

Nanoparticles have been incorporated with quantum dots, gold nanorods, magnetic and Gd-loaded silica nanoparticles into perfluorobutane microbubbles, which serve as an agent for optical, photoacoustic, and MR imaging. A novel static micromixer coaxial electrospray (MCE) system[167] fabricated with a polymethyl methacrylate (PMMA) sheet is applied to the synthesis of theranostic lipoplexes. The therapeutic and imaging reagents of theranostic lipoplexes are quantum dots and Cy5-labeled antisense oligodeoxynucleotides (Cy5-G3139), respectively. The microfluidic system has produced highly uniform nanoparticles with a polydispersity index as low as 0.024, and higher encapsulation efficiency of the payloads than those prepared *via* bulk synthesis. Lipoprotein nanoparticles incorporated with a hydrophilic drug, gold nanoparticles, magnetic nanoparticles, quantum dots, or fluorophores can be used for imaging by CT, MRI or fluorescence detection instruments. Fayad's group[168] has reconstituted lipoprotein nanoparticles by a microfluidic system in a single step (Fig. 7), and the nanoparticles have showed good performance for cancer therapy as well as diagnosis.

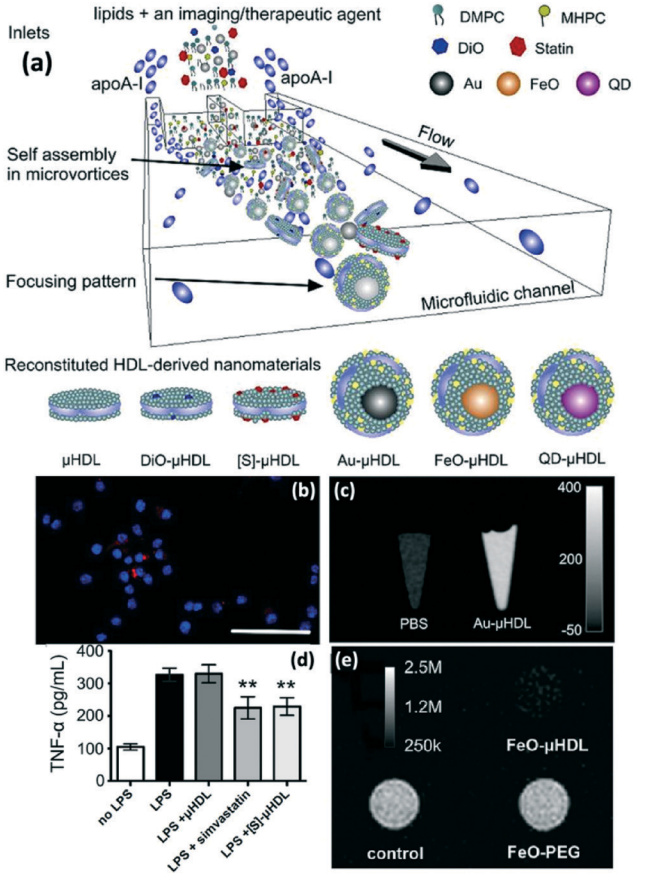

Fig. 7 (a) Scheme of a microfluidic platform for single-step and large-scale synthesis of a high-density lipoprotein (HDL): reconstituted HDL by microfluidics (μHDL); DiO-μHDL for fluorescence; [s]-μHDL for a therapeutic platform; Au-μHDL for CT imaging; FeO-μHDL for MRI; and QD-μHDL for fluorescence. (b) Confocal microscopy image of macrophages incubated with QD-μHDL. The scale bar is 100 μm. (c) CT imaging of PBS and Au-μHDL solutions. (d) [s]-μHDL for the delivery of hydrophobic molecules. (e) T_2-weighted MRI of macrophage cell pellets incubated with different solutions. Reproduced from ref. 168, copyright 2013 The American Chemical Society.

4. Conclusions and future perspectives

Continuous-flow microfluidic systems are widely studied for the synthesis of nanoparticles with a variety of attractive features, including precise control of reaction conditions, rapid mass and heat transfer, online characterization, quick feedback, safe operation, environmental friendliness and high scalability. Microfluidics has also proven to be a powerful platform to fabricate and optimize various nanoparticles including metal nanoparticles, oxide nanoparticles, semiconductors, organic nanoparticles, and hybrid organic–inorganic nanoparticle composites. The synthesized nanoparticles can be used for imaging, biosensing, drug delivery, and theranostic applications. Because of their capability to separate the nucleation and growth stages in nanoparticle formation, nanoparticles with higher uniformity and lower polydispersity index can be prepared within microfluidic platforms with enhanced performance in various applications. A list of nanoparticles is tabulated in Table 2 to facilitate comparison between their types, size, shape and the microfluidic platform required for nanosynthesis.

Serving as a nanofabrication platform, microfluidics has already demonstrated its synergistic effects in the field of biomedicine. Despite the great potential, more efforts should be devoted into on-chip synthesis. Firstly, many nanoparticles readily diffuse in the matrix of PDMS, thus other materials should be explored for the fabrication of cost-effective, robust, and reliable microdevices. Secondly, purification and extraction processes, which are easily achievable in conventional approaches, should be improved in microfluidic platforms. More efforts should be dedicated to integrate the nanoparticle synthesis, purification and extraction to realize fully automated production. Lastly, the integration and development of online analytical methods with the microfluidic approach will significantly improve the synthesis performance by optimizing processes with an immediate feedback control. With the integration of online and on demand characterization, microfluidics is expected to be a promising platform to optimize and tailor nanoparticles for different applications.

Table 2 Examples of nanoparticles synthesized in microfluidic platforms for biomedical applications

Phase	Substrate of microreactors	Materials		Reactants	Temp (°C)	Size	Shape	Potential biomedical applications		Year	Ref.
Single	Alloy (stainless steel)	Inorganic	Ag	Trioctylamine + silver pentafluoropropionate in isoamyl ether	100–140	3–12 nm	Spheres	Biosensing	Proof-of-concept	2004	53
Single	PDMS	Inorganic	Ag	$AgNO_3$ + hydroxylamine hydrochloride + NaOH	RT	10–20 nm	Cubes	Biosensing	Determination of the natural pigment scytonemin from cyanobacteria	2010	105
Single	Glass	Inorganic	Au	Thiolate oligomer or polymer + $HAuCl_4$ + $NaBH_4$	RT	3–4 nm	Spheres	Biosensing	LSPR	2007	113
Single	Hybrid (silicon–Pyrex)	Inorganic	Au	12 nm Au seeds + $HAuCl_4$ + ascorbic acid	RT	15–24 nm	Spheres	Biosensing	Proof-of-concept	2004	120
Single	Hybrid (silicon–Pyrex)	Inorganic	Au	$HAuCl_4$ + PVP + ascorbic acid	RT	5–50 nm	Spheres	Biosensing	Proof-of-concept	2005	29
Single	PDMS	Inorganic	Au	$HAuCl_4$/1-methylimidazole and $NaBH_4$ in BMIM-BF_4	RT	4.38 ± 0.53	Spheres	Biosensing	Bionanotechnology, chemical catalysis	2010	112
Single	PDMS	Inorganic	Au	Au seeds + $HAuCl_4$ + ascorbic acid + CTAC + NaBr	RT	50 nm	Supraparticles	Biosensing	Proof-of-concept	2015	26
Single	Thermoplastics (PE)	Inorganic	Au	Mercaptohexanoic acid/CTAB/ citrate + $HAuCl_4$ + $NaBH_4$ + $AgNO_3$ + ascorbic acid	RT	2–40 nm	Spheres, nanorods	Biosensing	Proof-of-concept	2013	106
Single	Thermoplastics (PEEK)	Inorganic	Au	Sodium citrate + $CoCl_2$ + PVP + $NaBH_4$ + $HAuCl_4$ + PEG	RT	40 nm	Hollow gold nanoparticles	Biosensing	Plasmonic functionalities	2014	111
Single	Thermoplastics (PEEK)	Inorganic	Au	$HAuCl_4$ + ascorbic acid + CTAB + $AgNO_3$ + $NaBH_4$	30	Diameter = 10 nm, length = 50–100 nm	Nanorods	Biosensing	Chemical sensing	2015	25
Single	Thermoplastics (PEEK)	Inorganic	Au	$HAuCl_4$ + ascorbic acid + CTAB + $AgNO_3$ + $NaBH_4$ + PEG-SH	RT	Diameter = 10–20 nm, length = 20–50 nm	Nanorods	Biosensing	Proof-of-concept	2016	107
Single	Glass or silicon	Inorganic	Au/Ag	$AgNO_3$/$HAuCl_4$ + $NaBH_4$	RT	4–7 nm	Spheres	Biosensing	Proof-of-concept	2008	108
Single	PDMS	Inorganic	$CoFe_2O_4$	$FeCl_3$ + $CoCl_2$ + TMAOH	98	6	Spheres	Imaging	MRI	2012	77
Single	Alloy (stainless steel)	Inorganic	Fe(B)@Fe_3O_4	$FeCl_2$ + PVP + $NaBH_4$ + H_2O	60–90	Core: 8–21 nm, shell:3–5 nm	Core–shell spheres	Imaging	MRI	2013	74
Single	PDMS	Inorganic	Fe_2O_3@SiO_2	γ-Fe_2O_3 + APTES + TEOS + RITC + NH_4OH	RT	50 nm	Spheres	Imaging	Fluorescence imaging + MRI	2009	48
Single	Alloy (Hastelloy)	Inorganic	Fe_3O_4	$Fe(acac)_3$ + oleylamine + HOOC–PEG–COOH + anisole	250	5–6 nm	Spheres	Imaging	MRI	2015	79

Table 2 *(continued)*

Phase	Substrate of microreactors	Materials		Reactants	Temp (°C)	Size	Shape	Potential biomedical applications		Year	Ref.
Single	PDMS	Inorganic	Fe_3O_4	$FeCl_3$ + $FeCl_2$ + TMAOH	RT	<7 nm	Spheres	Imaging	MRI	2008	71
Single	PDMS	Inorganic	Goethite	$FeCl_3$ + $FeCl_2$ + HCl + TMAOH	60	L = 30 ± 17; W = 7 ± 4 nm	Nanolaths	Imaging	MRI	2009	72
Single	Hybrid (silicon–Pyrex)	Inorganic	Pt	Pd acetate + oleylamine/trioctylphosphine	30–40	1 nm	Spheres	Biosensing	H_2 storage, separation and sensing	2015	96
Single	Thermoplastics (PTFE)	Inorganic	Silica–titania	TEOS + NH_4OH + TTIP + H_2O + IPA + ODA	RT	33 nm	Spheres	Biosensing	Humidity sensors	2015	85
Single	Glass	Inorganic	SiO_2–Au–Fe_2O_3	SiO_2–RITC + Au + γ-Fe_2O_3	RT	200 nm	Spheres	Imaging	Fluorescence imaging + MRI	2013	78
Single	Glass	Inorganic	$Zn_xFe_{3-x}O_4$	$FeCl_3$ + $FeCl_2$ + HCl + $ZnCl_2$ + NH_4OH	RT	<5 nm	Spheres	Imaging	MRI	2015	76
Single	PDMS	Organic	Chitosan/DNA	Chitosan + CpG ODN	RT	179–234 nm	Spheres	Drug delivery	Gene delivery	2014	159
Single	PDMS	Organic	Lipid	DLinKC2-DMA/DSPC/cholesterol PEG-*c*-DMA + siRNA	RT	70 nm	Spheres	Drug delivery	Gene delivery	2012	158
Single	Hybrid (PDMS–glass)	Organic	PDA	PCDA + DMSO + DI water	RT	36–84 nm	Spheres	Biosensing	Stimulus-induced fluorescence	2016	88
Single	PDMS	Organic	Polymer/DNA	Poly(2-hydroxypropyleneimine) + DNA	RT	200–263 nm	Spheres	Drug delivery	Gene delivery	2014	140
Single	Alloy (stainless steel)	Organic	Polymeric	CFA + acetone + isopropyl ether	5–50	350–1300 nm	Spheres	Drug delivery	Enhanced dissolution properties of CFA	2010	148
Single	Glass	Organic	Polymeric	PLGA + HPCS + AcDX + PTX	RT	70–280 nm	Spheres	Drug delivery	Anticancer	2015	40
Single	PDMS	Organic	Polymeric	PLGA–PEG + ACN + H_2O	RT	10–50 nm	Spheres	Drug delivery	Anticancer	2008	24
Single	PDMS	Organic	Polymeric	PLA–Pt(IV) + PLGA–PEG + PLA–Pt(IV) + docetaxel	RT	100 nm	Spheres	Drug delivery	Anticancer	2010	136
Single	PDMS	Organic	Polymeric	PLGA–PEG + PLGA + ACN + H_2O	RT	30–230 nm	Spheres	Drug delivery	Anticancer	2011	46
Single	PDMS	Organic	Polymeric	NIPAM + acrylamide + acrylic acid + NIPMAM + VP + DOX	8–45	60–120 nm	Spheres	Drug delivery	Anticancer	2012	138
Single	PDMS	Organic	Polymeric	PFE–PEG + THF + H_2O	RT	50–80 nm	Spheres	Imaging	Cell labeling	2012	143
Single	PDMS	Organic	Polymeric	Hydrophobically-modified chitosan + PTX in acid + basic water	RT	75–122 nm	Spheres	Drug delivery	Anticancer	2013	142
Single	PDMS	Organic	Polymeric	PLGA–PEG/PLGA–PEG–LIG/PLGA–Alexa488/PLGA–Alexa647 + ACN + H_2O	RT	25–200 nm	Spheres	Drug delivery	Anticancer	2013	144
Single	PDMS	Organic	Polymeric	PLGA–PEG + ACN + H_2O	RT	13–150 nm	Spheres	Drug delivery	Anticancer	2014	49
Single	PDMS	Organic	Polymeric	PLGA + ACN + H_2O	RT	55–135 nm	Spheres	Drug delivery	Anticancer	2014	147
Single	Thermoplastics (COC)	Organic	Polymeric	Folate–PEG–lipid + PEG–lipid	RT	70–115 nm	Spheres	Drug delivery	Target drug delivery	2013	135
Single	PDMS	Organic	Polymer–lipid	PLGA + DOX + SRF + Au + CD + DPPC + DSPE-PEG	RT	85 nm	Spheres	Theranostic	CT + fluorescence imaging + drug delivery	2013	169
Single	PDMS	Organic	Polymer–lipid	PLGA + DPPC + DSPE-PEG + cholesterol + DOX + CA4	RT	95–103 nm	Monolayer shells, lipid-	Drug delivery	Anticancer	2015	151

Table 2 *(continued)*

Phase	Substrate of microreactors	Materials		Reactants	Temp (°C)	Size	Shape	Potential biomedical applications		Year	Ref.
							bilayer shells				
Single	PDMS	Organic	Polymer–lipid	DPPC + DSPE-PEG + cholesterol + PLGA + DOTAP + DOX + siRNA	RT	130–150 nm	Nanovesicles	Drug delivery	Anticancer	2015	152
Single	Glass	Organic/ inorganic	Hybrid NPs	Psi + PEG-*b*-PHIS + PEG-*b*-PLA + sorafenib	RT	200–260 nm	Spheres	Drug delivery	Anticancer	2015	134
Single	Glass	Organic/ inorganic	Hybrid NPs	PTX + FSN + MTX + Psi + AcDX	RT	150–400 nm	Spheres	Drug delivery	Combination chemotherapy in breast cancer treatment	2015	139
Single	PDMS	Organic/ inorganic	Hybrid NPs	DMPC + MHPC + apoA-I + Au + FeO + QD + stain + DiO	RT	8–32 nm	Spheres	Theranostic	CT + MRI + drug delivery	2013	168
Single	PDMS	Organic/ inorganic	Hybrid NPs	PLGA /PLGA–BP + SPIO + PTX	RT	48–110 nm	Spheres	Theranostic	Bone-targeting, drug delivery and MRI for bone cancer	2015	170
Single	PDMS	Organic /inorganic	Hybrid vesicle	PS-*b*-PEO + PtNP + AuNR + RB	RT	388–2100 nm	Spheres	Drug delivery	Controlled release	2015	149
Single	Thermoplastics (PMMA)	Organic/ inorganic	Lipoplexes	QD605 + Cy5-G3139 + DOTAP + EggPC + DSPE-PEG	RT	194 ± 15 nm	Spheres	Theranostic	Cell imaging + gene delivery	2012	167
Single	PDMS	Organic/ inorganic	Polymer/Fe_3O_4	PEG-DA + acrylic acid + $FeCl_3$ + $FeCl_2$ + NaOH + NH_4OH	RT	3–5 nm by 20–300 μm	Disks, triangular Janus disks, gradient particles	Imaging	MRI	2012	73
Single	PDMS	Organic/ inorganic	Polymer–AuNRs	PEO45-*b*-PS211 + AuNRs + THF + H_2O	RT	0.5–2 μm	Giant vesicles	Drug delivery	Controlled release	2013	133
Multi	Glass	Inorganic	Ag	Diethylene glycol + NaSH + CF_3COOAg + PVP	RT	30–100 nm	Cubes, Octahedra	Biosensing	Molecular or biochip labeling	2013	102
Multi	Thermoplastics (PEEK)	Inorganic	Ag	Ag seeds + $C_6H_8O_6$ + $AgNO_3$	RT	35–180 nm	Nanoprisms	Biosensing	Molecular labeling	2012	59
Multi	Hybrid (silicon–Pyrex)	Inorganic	Au	$HAuCl_4$ + $NaBH_4$ + TTAB	100	3–15 nm	Spheres	Biosensing	LSPR	2012	60
Multi	PDMS	Inorganic	Au	Au seeds + $HAuCl_4$ + ascorbic acid + CTAB	35	10–100 nm	Spheres/spheroids, rods, sharp-edged structures	Biosensing	Optical resonances in the vis–NIR spectral range	2009	44
Multi	PDMS	Inorganic	Au	Gold-seeded silica particles + hydroxylamine hydrochloride + gold hydroxide	RT	Core 5–200 nm, shell 5 nm	Nanoshells	Biosensing	Plasmonics, chemical catalysis, optoelectronics, and biological sensing	2010	116
Multi	PDMS	Inorganic	Au	$HAuCl_4$ + $NaBH_4$ + CTAB	35	<5 nm	Spheres	Biosensing	Cytochemical probes	2012	111
Multi	Thermoplastics (PEEK)	Inorganic	Au	Au seeds + $HAuCl_4$ + ascorbic acid + CTAC	RT	15–50	Spheres, cubes	Biosensing	Photonics	2014	27
Multi	PDMS	Inorganic	Au/Ag	Au seeds + $HAuCl_4$ + ascorbic acid + CTAB + tetradecane + $AgNO_3$	RT/80	5–50 nm	Au/Ag core–shells, Au/Ag/Au double shells	Biosensing	Optical labelling	2011	57
Multi	PDMS	Inorganic	Au/Ag	$HAuCl_4$/$AgBF_4$ /1-methylimidazole + BMIM-BH_4 + BMIM-Tf_2N	RT	3–5 nm	Spheres	Biosensing	LSPR	2012	100
Multi	PDMS	Inorganic	Fe_3O_4	$FeCl_3$ + $FeCl_2$ + HCl + NH_4OH	RT	4 nm	Spheres	Imaging	MRI	2008	80
Multi	Thermoplastics (PEEK)	Inorganic	Pd	Na_2PdCl_4 + KCl/KBr + PVP	22–80	9–37 nm	Cuboctahedra, octahedra, cubes	Biosensing	Photonics	2014	27
Multi	Thermoplastics (PEEK)	Inorganic	Pd@Au	Pd cubes + $HAuCl_4$ + ascorbic acid + KBr + PVP	60	20 nm	Cubes	Biosensing	Photonics	2014	27

Table 2 *(continued)*

Phase	Substrate of microreactors	Materials		Reactants	Temp (°C)	Size	Shape	Potential biomedical applications		Year	Ref.
Multi	PDMS	Inorganic	SiO_2	FITC + APTES + TEOS + NH_4OH + H_2O + ethanol	RT	50–350 nm	Spheres	Imaging	Fluorescence imaging	2012	67
Multi	Thermoplastics (PMMA)	Organic	Lipid–PFC	DSPE-PEG2000 + C_4F_{10}	RT	100–200 nm	Spheres	Imaging	Ultrasound	2016	69
Multi	PDMS	Organic	Microbubble	CO_2 + lysozyme, alginate, and anionic NPs	RT	5 μm	Spheres	Imaging	Ultrasound + MRI	2010	82
Multi	PDMS	Organic	Polymer/gene/TFs	Ad–PEG + Ad–PEG–RGD + Ad–PEG–TAT + CD–PEI + BSA–Cy5 + HRP–RhB + pEGFP	RT	100–480 nm	Spheres	Drug delivery	Immunotherapy, stem cell reprogramming	2016	161
Multi	PDMS	Organic	Polymeric	PS-*b*-PAA + DMF/dioxane/water	RT	30–400 nm	Spheres, cylinders, vesicles	Drug delivery	Anticancer	2013	146
Multi	PDMS	Organic	Polymeric	PNBM-*b*-PEO + water/dioxane	RT	17–80 nm	Spheres, spool-like NPs	Drug delivery	Photoresponsive drug release	2015	150
Multi	Silicon	Organic	Polymeric	MMA + EGDMA + AIBN + PSS-*co*-PM + PSSS + PAES	97	30–600 nm	Ellipsoidal, dumbbell-like particles	Drug delivery	Anticancer	2014	145
Multi	PDMS	Organic	SMP	Ad–PAMAM + Ad–PEG + CD–PEI + RGD–PEG–Ad	RT	35–350 nm	Spheres	Imaging	Cell imaging	2010	68
Multi	PDMS	Organic/ inorganic	Hybrid NPs	PCL + PVA + CdTe + Fe_3O_4 + tamoxifen	RT	50–200 μm	Spheres	Theranostic	Magnetic targeting, fluorescence imaging and drug controlled release	2009	164
Multi	Glass	Organic/ inorganic	Polyacrylamide/ silver	$AgNO_3$ + $NaBH_4$ + ascorbic acid + acrylamide	RT	100 nm in 50 μm	Spheres	Biosensing	Single particle-based SERS for detection of adenine	2013	84

Acknowledgements

The work was supported by grants from the University of Macau (MYRG2014-00179-ICMS-QRCM and MYRG2016-00201-ICMS-QRCM) and Guangdong-Hong Kong Technology Cooperation Funding Scheme (2016A050503027).

References

1 U. Bilati, E. Allemann and E. Doelker, *Eur. J. Pharm. Sci.*, 2005, **24**, 67–75.
2 T. Govender, S. Stolnik, M. C. Garnett, L. Illum and S. S. Davis, *J. Controlled Release*, 1999, **57**, 171–185.
3 A. Kumari, S. K. Yadav and S. C. Yadav, *Colloids Surf., B*, 2010, **75**, 1–18.
4 C. Burda, X. B. Chen, R. Narayanan and M. A. El-Sayed, *Chem. Rev.*, 2005, **105**, 1025–1102.
5 S. Laurent, D. Forge, M. Port, A. Roch, C. Robic, L. V. Elst and R. N. Muller, *Chem. Rev.*, 2008, **108**, 2064–2110.
6 Y. Lu, Y. D. Yin, B. T. Mayers and Y. N. Xia, *Nano Lett.*, 2002, **2**, 183–186.
7 C. Liu, B. S. Zou, A. J. Rondinone and Z. J. Zhang, *J. Am. Chem. Soc.*, 2001, **123**, 4344–4345.
8 J. H. Bang and K. S. Suslick, *Adv. Mater.*, 2010, **22**, 1039–1059.
9 L. Sun, J. Li, C. L. Wang, S. F. Li, Y. K. Lai, H. B. Chen and C. J. Lin, *J. Hazard. Mater.*, 2009, **171**, 1045–1050.
10 S. Santra, R. Tapec, N. Theodoropoulou, J. Dobson, A. Hebard and W. H. Tan, *Langmuir*, 2001, **17**, 2900–2906.
11 X. J. Zhao, R. P. Bagwe and W. H. Tan, *Adv. Mater.*, 2004, **16**, 173–176.
12 A. J. Zarur and J. Y. Ying, *Nature*, 2000, **403**, 65–67.
13 M. A. Lopez-Quintela, *Curr. Opin. Colloid Interface Sci.*, 2003, **8**, 137–144.
14 N. R. Jana, L. Gearheart and C. J. Murphy, *Chem. Mater.*, 2001, **13**, 2313–2322.
15 Z. S. Pillai and P. V. Kamat, *J. Phys. Chem. B*, 2004, **108**, 945–951.
16 Y. Lee, J. R. Choi, K. J. Lee, N. E. Stott and D. Kim, *Nanotechnology*, 2008, **19**(41), 415604.
17 C. J. Murphy, T. K. San, A. M. Gole, C. J. Orendorff, J. X. Gao, L. Gou, S. E. Hunyadi and T. Li, *J. Phys. Chem. B*, 2005, **109**, 13857–13870.
18 H. Z. Wang, X. Y. Li, M. Uehara, Y. Yamaguchi, H. Nakamura, M. P. Miyazaki, H. Shimizu and H. Maeda, *Chem. Commun.*, 2004, 48–49.
19 E. M. Chan, A. P. Alivisatos and R. A. Mathies, *J. Am. Chem. Soc.*, 2005, **127**, 13854–13861.
20 S. Krishnadasan, R. J. C. Brown, A. J. deMello and J. C. deMello, *Lab Chip*, 2007, **7**, 1434–1441.
21 J. Dai, X. Y. Yang, M. Hamon and L. Z. Kong, *Chem. Eng. J.*, 2015, **280**, 385–390.
22 I. Lignos, S. Stavrakis, A. Kilaj and A. J. deMello, *Small*, 2015, **11**, 4009–4017.
23 J. Dai, X. Y. Yang, M. Hamon, L. Z. Kong, W. S. Lee, S. Park and J. W. Hong, *Chem. Eng. J.*, 2016, **286**, 347.
24 R. Karnik, F. Gu, P. Basto, C. Cannizzaro, L. Dean, W. Kyei-Manu, R. Langer and O. C. Farokhzad, *Nano Lett.*, 2008, **8**, 2906–2912.
25 J. Watt, B. G. Hance, R. S. Anderson and D. L. Huber, *Chem. Mater.*, 2015, **27**, 6442–6449.
26 Q. Fu, Y. Sheng, H. Tang, Z. Zhu, M. Ruan, W. Xu, Y. Zhu and Z. Tang, *ACS Nano*, 2015, **9**, 172–179.
27 L. Zhang, G. D. Niu, N. Lu, J. G. Wang, L. M. Tong, L. D. Wang, M. J. Kim and Y. N. Xia, *Nano Lett.*, 2014, **14**, 6626–6631.
28 J. Angly, A. Iazzolino, J. B. Salmon, J. Leng, S. P. Chandran, V. Ponsinet, A. Desert, A. Le Beulze, S. Mornet, M. Treguer-Delapierre and M. A. Correa-Duarte, *ACS Nano*, 2013, **7**, 6465–6477.
29 J. Wagner and J. M. Kohler, *Nano Lett.*, 2005, **5**, 685–691.
30 K. S. Krishna, Y. H. Li, S. N. Li and C. S. S. R. Kumar, *Adv. Drug Delivery Rev.*, 2013, **65**, 1470–1495.
31 S. Marre and K. F. Jensen, *Chem. Soc. Rev.*, 2010, **39**, 1183–1202.
32 A. Abou-Hassan, O. Sandre and V. Cabuil, *Angew. Chem., Int. Ed.*, 2010, **49**, 6268–6286.
33 Y. Song, J. Hormes and C. S. Kumar, *Small*, 2008, **4**, 698–711.
34 G. Niu, A. Ruditskiy, M. Vara and Y. Xia, *Chem. Soc. Rev.*, 2015, **44**, 5806–5820.
35 P. W. Dunne, A. S. Munn, C. L. Starkey, T. A. Huddle and E. H. Lester, *Philos. Trans. R. Soc., A*, 2015, **373**(2057), 20150015.
36 I. U. Khan, C. A. Serra, N. Anton and T. Vandamme, *J. Controlled Release*, 2013, **172**, 1065–1074.
37 C.-X. Zhao, L. He, S. Z. Qiao and A. P. J. Middelberg, *Chem. Eng. Sci.*, 2011, **66**, 1463–1479.
38 S. Q. Xu, Z. H. Nie, M. Seo, P. Lewis, E. Kumacheva, H. A. Stone, P. Garstecki, D. B. Weibel, I. Gitlin and G. M. Whitesides, *Angew. Chem., Int. Ed.*, 2005, **44**, 724–728.
39 J. B. Edel, R. Fortt, J. C. deMello and A. J. deMello, *Chem. Commun.*, 2002, 1136–1137.
40 D. F. Liu, S. Cito, Y. Z. Zhang, C. F. Wang, T. M. Sikanen and H. A. Santos, *Adv. Mater.*, 2015, **27**, 2298–2304.
41 H. Nakamura, A. Tashiro, Y. Yamaguchi, M. Miyazaki, T. Watari, H. Shimizu and H. Maeda, *Lab Chip*, 2004, **4**, 237–240.
42 P. M. Valencia, O. C. Farokhzad, R. Karnik and R. Langer, *Nat. Nanotechnol.*, 2012, **7**, 623–629.
43 J. I. Park, A. Saffari, S. Kumar, A. Günther and E. Kumacheva, *Annu. Rev. Mater. Res.*, 2010, **40**, 415–443.
44 S. Duraiswamy and S. A. Khan, *Small*, 2009, **5**, 2828–2834.
45 J. Kobayashi, Y. Mori, K. Okamoto, R. Akiyama, M. Ueno, T. Kitamori and S. Kobayashi, *Science*, 2004, **304**, 1305–1308.
46 M. Rhee, P. M. Valencia, M. I. Rodriguez, R. Langer, O. C. Farokhzad and R. Karnik, *Adv. Mater.*, 2011, **23**, H79–H83.
47 G. J. Liu, X. H. Yang, Y. Li, Z. G. Yang, W. Hong and J. F. Liu, *Adv. Mater. Sci. Eng.*, 2015, **10**(1155), 160819.
48 A. Abou-Hassan, R. Bazzi and V. Cabuil, *Angew. Chem., Int. Ed.*, 2009, **48**, 7180–7183.
49 J. M. Lim, N. Bertrand, P. M. Valencia, M. Rhee, R. Langer, S. Jon, O. C. Farokhzad and R. Karnik, *Nanomedicine*, 2014, **10**, 401–409.

50 T. J. Johnson, D. Ross and L. E. Locascio, *Anal. Chem.*, 2002, **74**, 45–51.
51 V. Hessel, H. Lowe and F. Schonfeld, *Chem. Eng. Sci.*, 2005, **60**, 2479–2501.
52 A. D. Stroock, S. K. Dertinger, A. Ajdari, I. Mezic, H. A. Stone and G. M. Whitesides, *Science*, 2002, **295**, 647–651.
53 Z. L. Xue, A. D. Terepka and Y. Hong, *Nano Lett.*, 2004, **4**, 2227–2232.
54 A. Gunther and K. F. Jensen, *Lab Chip*, 2006, **6**, 1487–1503.
55 L. Shui, J. C. T. Eijkel and A. van den Berg, *Adv. Colloid Interface Sci.*, 2007, **133**, 35–49.
56 H. Song, D. L. Chen and R. F. Ismagilov, *Angew. Chem., Int. Ed.*, 2006, **45**, 7336–7356.
57 A. Knauer, A. Thete, S. Li, H. Romanus, A. Csaki, W. Fritzsche and J. M. Kohler, *Chem. Eng. J.*, 2011, **166**, 1164–1169.
58 D. R. Kumar, B. Prasad and A. Kulkarni, *Chem. Eng. J.*, 2012, **192**, 357–368.
59 A. Knauer, A. Csaki, F. Moller, C. Huhn, W. Fritzsche and J. M. Kohler, *J. Phys. Chem. C*, 2012, **116**, 9251–9258.
60 V. S. Cabeza, S. Kuhn, A. A. Kulkarni and K. F. Jensen, *Langmuir*, 2012, **28**, 7007–7013.
61 J. C. Baret, *Lab Chip*, 2012, **12**, 422–433.
62 B. K. H. Yen, A. Gunther, M. A. Schmidt, K. F. Jensen and M. G. Bawendi, *Angew. Chem., Int. Ed.*, 2005, **44**, 5447–5451.
63 A. Gunther, M. Jhunjhunwala, M. Thalmann, M. A. Schmidt and K. F. Jensen, *Langmuir*, 2005, **21**, 1547–1555.
64 Z. Yu, O. Heraminger and L. S. Fan, *Chem. Eng. Sci.*, 2007, **62**, 7172–7183.
65 A. Gunther, S. A. Khan, M. Thalmann, F. Trachsel and K. F. Jensen, *Lab Chip*, 2004, **4**, 278–286.
66 S. A. Khan and K. F. Jensen, *Adv. Mater.*, 2007, **19**, 2556–2560.
67 J. B. Wacker, I. Lignos, V. K. Parashar and M. A. M. Gijs, *Lab Chip*, 2012, **12**, 3111–3116.
68 K. Liu, H. Wang, K. J. Chen, F. Guo, W. Y. Lin, Y. C. Chen, D. L. Phung, H. R. Tseng and C. K. F. Shen, *Nanotechnology*, 2010, **21**(44), 445603.
69 S. A. Peyman, J. R. McLaughlan, R. H. Abou-Saleh, G. Marston, B. R. G. Johnson, S. Freear, P. L. Coletta, A. F. Markham and S. D. Evans, *Lab Chip*, 2016, **16**, 679–687.
70 U. I. Tromsdorf, N. C. Bigall, M. G. Kaul, O. T. Bruns, M. S. Nikolic, B. Mollwitz, R. A. Sperling, R. Reimer, H. Hohenberg, W. J. Parak, S. Forster, U. Beisiegel, G. Adam and H. Weller, *Nano Lett.*, 2007, **7**, 2422–2427.
71 A. Abou Hassan, O. Sandre, V. Cabuil and P. Tabeling, *Chem Commun.*, 2008, 1783–1785.
72 A. Abou-Hassan, O. Sandre, S. Neveu and V. Cabuil, *Angew. Chem., Int. Ed.*, 2009, **48**, 2342–2345.
73 S. K. Suh, K. Yuet, D. K. Hwang, K. W. Bong, P. S. Doyle and T. A. Hatton, *J. Am. Chem. Soc.*, 2012, **134**, 7337–7343.
74 Y. J. Song, S. X. Ji, Y. J. Song, R. S. Li, J. Ding, X. M. Shen, R. M. Wang, R. W. Xu and X. Y. Gu, *J. Phys. Chem. C*, 2013, **117**, 17274–17284.
75 F. C. Cabrera, A. F. Melo, J. C. de Souza, A. E. Job and F. N. Crespilho, *Lab Chip*, 2015, **15**, 1835–1841.
76 M. D. Simmons, N. Jones, D. J. Evans, C. Wiles, P. Watts, S. Salamon, M. E. Castillo, H. Wende, D. C. Lupascu and M. G. Francesconi, *Lab Chip*, 2015, **15**, 3154–3162.
77 A. Abou-Hassan, S. Neveu, V. Dupuis and V. Cabuil, *RSC Adv.*, 2012, **2**, 11263–11266.
78 N. Hassan, V. Cabuil and A. Abou-Hassan, *Angew. Chem., Int. Ed.*, 2013, **52**, 1994–1997.
79 M. X. Jiao, J. F. Zeng, L. H. Jing, C. Y. Liu and M. Y. Gao, *Chem. Mater.*, 2015, **27**, 1299–1305.
80 L. Frenz, A. El Harrak, M. Pauly, S. Begin-Colin, A. D. Griffiths and J. C. Baret, *Angew. Chem., Int. Ed.*, 2008, **47**, 6817–6820.
81 I. Lignos, S. Stavrakis, G. Nedelcu, L. Protesescu, A. J. Demello and M. V. Kovalenko, *Nano Lett.*, 2016, **16**, 1869–1877.
82 J. I. Park, D. Jagadeesan, R. Williams, W. Oakden, S. Chung, G. J. Stanisz and E. Kumacheva, *ACS Nano*, 2010, **4**, 6579–6586.
83 N. Visaveliya, S. Lenke and J. M. Kohler, *ACS Appl. Mater. Interfaces*, 2015, **7**, 10742–10754.
84 J. M. Koher, A. Marz, J. Popp, A. Knauer, I. Kraus, J. Faerber and C. Serra, *Anal. Chem.*, 2013, **85**, 313–318.
85 K. Shiba, T. Sugiyama, T. Takei and G. Yoshikawa, *Chem Commun.*, 2015, **51**, 15854–15857.
86 J. Parisi, L. Su and Y. Lei, *Lab Chip*, 2013, **13**, 1501–1508.
87 M. R. Alenezi, S. J. Henley and S. R. P. Silva, *Sci. Rep.*, 2015, **5**, 8516.
88 S. Baek, S. Song, J. Lee and J.-M. Kim, *Sens. Actuators, B*, 2016, **230**, 623–629.
89 M. W. Ahn, K. S. Park, J. H. Heo, D. W. Kim, K. J. Choi and J. G. Park, *Sens. Actuators, B*, 2009, **138**, 168–173.
90 N. D. Khoang, H. S. Hong, D. D. Trung, N. Van Duy, N. D. Hoa, D. D. Thinh and N. Van Hieu, *Sens. Actuators, B*, 2013, **181**, 529–536.
91 V. T. Le, D. H. Nguyen, T. T. L. Dang, T. V. Do, D. T. Phuong, A. T. Le and V. H. Nguyen, *Sens. Actuators, B*, 2010, **146**, 361–367.
92 K. Saha, S. S. Agasti, C. Kim, X. Li and V. M. Rotello, *Chem. Rev.*, 2012, **112**, 2739–2779.
93 E. Boisselier and D. Astruc, *Chem. Soc. Rev.*, 2009, **38**, 1759–1782.
94 L. Dykman and N. Khlebtsov, *Chem. Soc. Rev.*, 2012, **41**, 2256–2282.
95 S. Zeng, K.-T. Yong, I. Roy, X.-Q. Dinh, X. Yu and F. Luan, *Plasmonics*, 2011, **6**, 491–506.
96 A. M. Karim, N. Al Hasan, S. Ivanov, S. Siefert, R. T. Kelly, N. G. Hallfors, A. Benavidez, L. Kovarik, A. Jenkins, R. E. Winans and A. K. Datye, *J. Phys. Chem. C*, 2015, **119**, 13257–13267.
97 M. E. Stewart, C. R. Anderton, L. B. Thompson, J. Maria, S. K. Gray, J. A. Rogers and R. G. Nuzzo, *Chem. Rev.*, 2008, **108**, 494–521.
98 V. Giannini, A. I. Fernandez-Dominguez, S. C. Heck and S. A. Maier, *Chem. Rev.*, 2011, **111**, 3888–3912.
99 L. A. Lyon, M. D. Musick and M. J. Natan, *Anal. Chem.*, 1998, **70**, 5177–5183.

100 L. L. Lazarus, C. T. Riche, B. C. Marin, M. Gupta, N. Malmstadt and R. L. Brutchey, *ACS Appl. Mater. Interfaces*, 2012, **4**, 3077–3083.
101 G. A. Patil, M. L. Bari, B. A. Bhanvase, V. Ganvir, S. Mishra and S. H. Sonawane, *Chem. Eng. Process.*, 2012, **62**, 69–77.
102 L. Zhang, Y. Wang, L. M. Tong and Y. N. Xia, *Langmuir*, 2013, **29**, 15719–15725.
103 R. Baber, L. Mazzei, N. T. K. Thanh and A. Gavriilidis, *RSC Adv.*, 2015, **5**, 95585–95591.
104 J. Puigmarti-Luis, M. Rubio-Martinez, I. Imaz, B. Z. Cvetkovic, L. Abad, A. Perez Del Pino, D. Maspoch and D. B. Amabilino, *ACS Nano*, 2014, **8**, 818–826.
105 R. Wilson, S. A. Bowden, J. Parnell and J. M. Cooper, *Anal. Chem.*, 2010, **82**, 2119–2123.
106 S. E. Lohse, J. R. Eller, S. T. Sivapalan, M. R. Plews and C. J. Murphy, *ACS Nano*, 2013, **7**, 4135–4150.
107 L. Uson, V. Sebastian, M. Arruebo and J. Santamaria, *Chem. Eng. J.*, 2016, **285**, 286–292.
108 J. Wagner, T. R. Tshikhudo and J. M. Koehler, *Chem. Eng. J.*, 2008, **135**, S104–S109.
109 C. H. Weng, C. C. Huang, C. S. Yeh, H. Y. Lei and G. B. Lee, *J. Micromech. Microeng.*, 2008, **18**(3), 035019.
110 L. Gomez, V. Sebastian, S. Irusta, A. Ibarra, M. Arruebo and J. Santamaria, *Lab Chip*, 2014, **14**, 325–332.
111 S. A. Khan and S. Duraiswamy, *Lab Chip*, 2012, **12**, 1807–1812.
112 L. L. Lazarus, A. S. J. Yang, S. Chu, R. L. Brutchey and N. Malmstadt, *Lab Chip*, 2010, **10**, 3377–3379.
113 D. Shalom, R. C. R. Wootton, R. F. Winkle, B. F. Cottam, R. Vilar, A. J. deMello and C. P. Wilde, *Mater. Lett.*, 2007, **61**, 1146–1150.
114 K. Sugano, Y. Uchida, O. Ichihashi, H. Yamada, T. Tsuchiya and O. Tabata, *Microfluid. Nanofluid.*, 2010, **9**, 1165–1174.
115 S. Y. Yang, F. Y. Cheng, C. S. Yeh and G. B. Lee, *Microfluid. Nanofluid.*, 2010, **8**, 303–311.
116 S. Duraiswamy and S. A. Khan, *Nano Lett.*, 2010, **10**, 3757–3763.
117 S. Gomez-de Pedro, M. Puyol and J. Alonso-Chamarro, *Nanotechnology*, 2010, **21**(41), 415603.
118 M. L. Personick and C. A. Mirkin, *J. Am. Chem. Soc.*, 2013, **135**, 18238–18247.
119 S. E. Lohse and C. J. Murphy, *Chem. Mater.*, 2013, **25**, 1250–1261.
120 J. Wagner, T. Kirner, G. Mayer, J. Albert and J. M. Kohler, *Chem. Eng. J.*, 2004, **101**, 251–260.
121 H. SadAbadi, S. Badilescu, M. Packirisamy and R. Wuthrich, *Biosens. Bioelectron.*, 2013, **44**, 77–84.
122 M. Lu, S. Yang, Y. P. Ho, C. L. Grigsby, K. W. Leong and T. J. Huang, *ACS Nano*, 2014, **8**, 10026–10034.
123 L. Xu, J. H. Peng, C. Srinivasakannan, L. B. Zhang, D. Zhang, C. H. Liu, S. X. Wang and A. Q. Shen, *RSC Adv.*, 2014, **4**, 25155–25159.
124 Z. L. Wang, *J. Phys.: Condens. Matter*, 2004, **16**, R829–R858.
125 A. Janotti and C. G. Van de Walle, *Rep. Prog. Phys.*, 2009, **72**(12), 126501.
126 Z. P. Sun, L. Liu, L. Zhang and D. Z. Jia, *Nanotechnology*, 2006, **17**, 2266–2270.
127 Y. Jin, J. Wang, B. Sun, J. C. Blakesley and N. C. Greenham, *Nano Lett.*, 2008, **8**, 1649–1653.
128 K. S. Soppimath, T. M. Aminabhavi, A. R. Kulkarni and W. E. Rudzinski, *J. Controlled Release*, 2001, **70**, 1–20.
129 J. Panyam and V. Labhasetwar, *Adv. Drug Delivery Rev.*, 2003, **55**, 329–347.
130 N. Anton, F. Bally, C. A. Serra, A. Ali, Y. Arntz, Y. Mely, M. J. Zhao, E. Marchioni, A. Jakhmola and T. F. Vandamme, *Soft Matter*, 2012, **8**, 10628–10635.
131 L. Chronopoulou, C. Sparago and C. Palocci, *J. Nanopart. Res.*, 2014, **16**(11), 1–10.
132 Q. Feng, L. Zhang, C. Liu, X. Y. Li, G. Q. Hu, J. S. Sun and X. Y. Jiang, *Biomicrofluidics*, 2015, **9**(5), 052604.
133 J. He, Z. J. Wei, L. Wang, Z. Tomova, T. Babu, C. Y. Wang, X. J. Han, J. T. Fourkas and Z. H. Nie, *Angew. Chem., Int. Ed.*, 2013, **52**, 2463–2468.
134 B. Herranz-Blanco, D. F. Liu, E. Makila, M. A. Shahbazi, E. Ginestar, H. B. Zhang, V. Aseyev, V. Balasubramanian, J. Salonen, J. Hirvonen and H. A. Santos, *Adv. Funct. Mater.*, 2015, **25**, 1488–1497.
135 R. R. Hood, C. R. Shao, D. M. Omiatek, W. N. Vreeland and D. L. DeVoe, *Pharm. Res.*, 2013, **30**, 1597–1607.
136 N. Kolishetti, S. Dhar, P. M. Valencia, L. Q. Lin, R. Karnik, S. J. Lippard, R. Langer and O. C. Farokhzad, *Proc. Natl. Acad. Sci. U. S. A.*, 2010, **107**, 17939–17944.
137 I. Kucuk and M. Edirisinghe, *Jom*, 2015, **67**, 811–817.
138 M. P. Leal, A. Torti, A. Riedinger, R. La Fleur, D. Petti, R. Cingolani, R. Bertacco and T. Pellegrino, *ACS Nano*, 2012, **6**, 10535–10545.
139 D. Liu, H. Zhang, E. Makila, J. Fan, B. Herranz-Blanco, C. F. Wang, R. Rosa, A. J. Ribeiro, J. Salonen, J. Hirvonen and H. A. Santos, *Biomaterials*, 2015, **39**, 249–259.
140 M. Lu, Y. P. Ho, C. L. Grigsby, A. A. Nawaz, K. W. Leong and T. J. Huang, *ACS Nano*, 2014, **8**, 332–339.
141 M. Maeki, T. Saito, Y. Sato, T. Yasui, N. Kaji, A. Ishida, H. Tani, Y. Baba, H. Harashima and M. Tokeshi, *RSC Adv.*, 2015, **5**, 46181–46185.
142 F. S. Majedi, M. M. Hasani-Sadrabadi, S. H. Emami, M. A. Shokrgozar, J. J. VanDersarl, E. Dashtimoghadam, A. Bertsch and P. Renaud, *Lab Chip*, 2013, **13**, 204–207.
143 F. Schutze, B. Stempfle, C. Jungst, D. Woll, A. Zumbusch and S. Mecking, *Chem. Commun.*, 2012, **48**, 2104–2106.
144 P. M. Valencia, E. M. Pridgen, M. Rhee, R. Langer, O. C. Farokhzad and R. Karnik, *ACS Nano*, 2013, **7**, 10671–10680.
145 N. Visaveliya and J. M. Kohler, *ACS Appl. Mater. Interfaces*, 2014, **6**, 11254–11264.
146 C. W. Wang, D. Sinton and M. G. Moffitt, *ACS Nano*, 2013, **7**, 1424–1436.
147 J. D. Wang, W. W. Chen, J. S. Sun, C. Liu, Q. F. Yin, L. Zhang, Y. L. Xianyu, X. H. Shi, G. Q. Hu and X. Y. Jiang, *Lab Chip*, 2014, **14**, 1673–1677.
148 J. X. Wang, Q. X. Zhang, Y. Zhou, L. Shao and J. F. Chen, *Chem. Eng. J.*, 2010, **162**, 844–851.

149 L. Wang, Y. J. Liu, J. He, M. J. Hourwitz, Y. L. Yang, J. T. Fourkas, X. J. Han and Z. H. Nie, *Small*, 2015, **11**, 3762–3767.
150 Z. Q. Xu, B. Yan, J. Riordon, Y. Zhao, D. Sinton and M. G. Moffitt, *Chem. Mater.*, 2015, **27**, 8094–8104.
151 L. Zhang, Q. Feng, J. L. Wang, S. Zhang, B. Q. Ding, Y. J. Wei, M. D. Dong, J. Y. Ryu, T. Y. Yoon, X. H. Shi, J. S. Sun and X. Y. Jiang, *ACS Nano*, 2015, **9**, 9912–9921.
152 L. Zhang, Q. Feng, J. Wang, J. Sun, X. Shi and X. Jiang, *Angew. Chem., Int. Ed.*, 2015, **54**, 3952–3956.
153 D. Chen, K. T. Love, Y. Chen, A. A. Eltoukhy, C. Kastrup, G. Sahay, A. Jeon, Y. Dong, K. A. Whitehead and D. G. Anderson, *J. Am. Chem. Soc.*, 2012, **134**, 6948–6951.
154 R. Riahi, A. Tamayol, S. A. M. Shaegh, A. M. Ghaemmaghami, M. R. Dokmeci and A. Khademhosseini, *Curr. Opin. Chem. Eng.*, 2015, **7**, 101–112.
155 Q. Feng, J. Sun and X. Jiang, *Nanoscale*, 2016, **8**, 12430–12443.
156 L. Zhang, J. M. Chan, F. X. Gu, J.-W. Rhee, A. Z. Wang, A. F. Radovic-Moreno, F. Alexis, R. Langer and O. C. Farokhzad, *ACS Nano*, 2008, **2**, 1696–1702.
157 E. Cohen-Sela, M. Chorny, N. Koroukhov, H. D. Danenberg and G. Golomb, *J. Controlled Release*, 2009, **133**, 90–95.
158 N. M. Belliveau, J. Huft, P. J. C. Lin, S. Chen, A. K. K. Leung, T. J. Leaver, A. W. Wild, J. B. Lee, R. J. Taylor, Y. K. Tam, C. L. Hansen and P. R. Cullis, *Mol. Ther.–Nucleic Acids*, 2012, **1**(8), e37.
159 S. Chen, H. J. Zhang, X. T. Shi, H. K. Wu and N. Hanagata, *Lab Chip*, 2014, **14**, 1842–1849.
160 J. G. Slagter-Jager, C. A. Nicolette and I. Y. Tcherepanova, *J. Pharm. Biomed. Anal.*, 2012, **70**, 657–663.
161 Y. Liu, J. Du, J. S. Choi, K. J. Chen, S. Hou, M. Yan, W. Y. Lin, K. S. Chen, T. Ro, G. S. Lipshutz, L. Wu, L. Shi, Y. Lu, H. R. Tseng and H. Wang, *Angew. Chem., Int. Ed.*, 2016, **55**, 169–173.
162 S. M. Janib, A. S. Moses and J. A. MacKay, *Adv. Drug Delivery Rev.*, 2010, **62**, 1052–1063.
163 J. Xie, S. Lee and X. Chen, *Adv. Drug Delivery Rev.*, 2010, **62**, 1064–1079.
164 C. H. Yang, K. S. Huang, Y. S. Lin, K. Lu, C. C. Tzeng, E. C. Wang, C. H. Lin, W. Y. Hsu and J. Y. Chang, *Lab Chip*, 2009, **9**, 961–965.
165 S. H. Hu and X. H. Gao, *J. Am. Chem. Soc.*, 2010, **132**, 7234–7237.
166 M. Seo, I. Gorelikov, R. Williams and N. Matsuura, *Langmuir*, 2010, **26**, 13855–13860.
167 Y. Wu, L. Li, Y. C. Mao and L. J. Lee, *ACS Nano*, 2012, **6**, 2245–2252.
168 Y. Kim, F. Fay, D. P. Cormode, B. L. Sanchez-Gaytan, J. Tang, E. J. Hennessy, M. M. Ma, K. Moore, O. C. Farokhzad, E. A. Fisher, W. J. M. Mulder, R. Langer and Z. A. Fayad, *ACS Nano*, 2013, **7**, 9975–9983.
169 A. J. Mieszawska, Y. Kim, A. Gianella, I. van Rooy, B. Priem, M. P. Labarre, C. Ozcan, D. P. Cormode, A. Petrov, R. Langer, O. C. Farokhzad, Z. A. Fayad and W. J. M. Mulder, *Bioconjugate Chem.*, 2013, **24**, 1429–1434.
170 M. M. Hasani-Sadrabadi, E. Dashtimoghadam, G. Bahlakeh, F. S. Majedi, H. Keshvari, J. J. Van Dersarl, A. Bertsch, A. Panahifar, P. Renaud, L. Tayebi, M. Mahmoudi and K. I. Jacob, *Nanomedicine*, 2015, **10**, 3431–3449.

